Research and Development

of a Small - Scale Adsorption Cooling System

by

Yeshpal Gupta

A Dissertation Presented in Partial Fulfillment
of the Requirements for the Degree
Doctor of Philosophy

Approved November 2011 by the
Graduate Supervisory Committee:

Patrick E Phelan, Chair
Harvey J Bryan
Pavlos G Mikellidas
Jose R Pacheco
Steven W Trimble

ARIZONA STATE UNIVERSITY

December 2011

ABSTRACT

The world is grappling with two serious issues related to energy and climate change. The use of solar energy is receiving much attention due to its potential as one of the solutions. Air conditioning is particularly attractive as a solar energy application because of the near coincidence of peak cooling loads with the available solar power.

Recently, researchers have started serious discussions of using adsorptive processes for refrigeration and heat pumps. There is some success for the >100 ton adsorption systems but none exists in the <10 ton size range required for residential air conditioning. There are myriad reasons for the lack of small-scale systems such as low Coefficient of Performance (COP), high capital cost, scalability, and limited performance data. A numerical model to simulate an adsorption system was developed and its performance was compared with similar thermal-powered systems. Results showed that both the adsorption and absorption systems provide equal cooling capacity for a driving temperature range of 70-120 ^{o}C, but the adsorption system is the only system to deliver cooling at temperatures below 65 ^{o}C. Additionally, the absorption and desiccant systems provide better COP at low temperatures, but the COP's of the three systems converge at higher regeneration temperatures. To further investigate the viability of solar-powered heat pump systems, an hourly building load simulation was developed for a single-family house in the Phoenix metropolitan area. Thermal as well as economic performance comparison

was conducted for adsorption, absorption, and solar photovoltaic (PV) powered vapor compression systems for a range of solar collector area and storage capacity. The results showed that for a small collector area, solar PV is more cost-effective whereas adsorption is better than absorption for larger collector area. The optimum solar collector area and the storage size were determined for each type of solar system. As part of this dissertation work, a small-scale proof-of-concept prototype of the adsorption system was assembled using some novel heat transfer enhancement strategies. Activated carbon and butane was chosen as the adsorbent-refrigerant pair. It was found that a COP of 0.12 and a cooling capacity of 89.6 W can be achieved.

I would like to thank my family, specially my wife Nidhi Gupta and my parents, for providing an abundance of love, encouragement, and support throughout the years of my pursuit of the doctoral degree.

ACKNOWLEDGEMENTS

First and foremost, I would like to dedicate special thanks to my advisor, Prof. Patrick Phelan, who has provided considerable wealth of resources, opportunities and guidance during my study of adsorption air conditioning systems. His support has been an essential contributing factor towards the completion of this manuscript. I would also like to thank the rest of my committee, Prof. Harvey Bryan, Dr. Pavlos Mikellidas, Dr. Jose Pacheco, and Prof. Steven Trimble, who have been very generous with their time and insights. I am also highly thankful to Mr. Jon Sherbeck who helped me on various aspects of the experimental system set-up and performing the experiment.

My stay at ASU has been made so unforgettable and enjoyable by all the people I have worked with through these years. I am indebted to Dr. Lynn Cozort, Moya Gilchrist, and Dr. Sharon Yee for their generous assistance. I would like to thank Dr. Bruce Steele, Wei-Yun Lai, Lionel Metchop, Brent Odom, Todd Otanicar, Rob Taylor, Himanshu Tyagi, and Sabarish Vinod for their friendship and technical support. I would also like to thank my supervisor Mr. Jorj Nofal at Lincus, Inc. for his continuous support and encouragement. Last but not least, I would like to thank my colleagues at Lincus, Inc. for their unconditional support throughout this arduous but fruitful journey.

I am grateful for the financial support from Edson Student Entrepreneur Initiative, ASU Graduate Professional Student Association,

University Graduate Fellowship, and Graduate Research and Teaching Assistantships.

TABLE OF CONTENTS

Page

CHAPTER Page

CHAPTER Page

APPENDIX

LIST OF FIGURES

Figure Page

Figure Page

LIST OF TABLES

NOMENCLATURE

$a0$	Zero-loss efficiency coefficient for thermal collector [-]
$a1$	1st order heat loss coefficient for thermal collector [-]
$a2$	2nd order heat loss coefficient for thermal collector [-]
A	Area [m^2]
b	Langmuir constant [-]
B	Temperature independent coefficient [-]
C	Specific heat [J kg^{-1} K^{-1}]
CI	Initial cost [$]
CO	Operating cost [$]
C_p	Specific heat at constant pressure [J kg^{-1} K^{-1}]
COP	Coefficient of performance [-]
d_f	DC to AC derate factor [-]
EAC	Equivalent annual cost [$]
DOD	Depth of discharge
EF	Energy factor [-]
E_x	Exergy capacity [Wh]
GC	Unit gas cost [$ $therm^{-1}$]
h	Enthalpy [J kg^{-1}]
H	Isosteric heat of adsorption [J kg^{-1}]
$HSPF$	Heating seasonal performance factor
I_t	Total solar radiation [W m^{-2}]
k	Constant [-]
k_B	Boltzmann constant [-]
$\dot{m}$	Mass flow rate [kg s^{-1}]
M	Mass [kg]
N	Useful life span [years]
p, P	Pressure [Pa]
q	Amount adsorbed [-]
q^{∞}	Limiting amount adsorbed [-]
$\dot{Q}$	Hear transfer rate [W]
r	Interest rate [-]
$SEER$	Seasonal energy efficiency ratio [-]
SF	Solar fraction [-]
t	time [s]
t_{cycle}	Cycle time [s]
T	Temperature [K]
T_o	Reference ambient temperature [K]
U	Overall heat transfer coefficient [W m^{-2} K^{-1}]
V	Volume [m^3]

Greek Symbols

ε	Regenerator effectiveness [-]
η	Efficiency [-]

ρ	Density [kg m^{-3}]

Subscripts

a	Ambient
ad	Adsorbent
ads	Adsorber
am	Adsorber material
aux	Auxiliary
av	Available
batt	Electric battery
c	Condenser
e	Evaporator
f	Liquid
gen	Generator
gh	Gas heater
hp	Vapor compression system heat pump
in	Inlet
inv	Electric inverter
m	Mean
max	Maximum
min	Minimum
out	Outlet
pv	Photovoltaic collector
ref	Refrigerant, Refrigeration
reg	Regenerator
req	Required
s	Storage
sat	Saturation
spv	Solar photovoltaic air conditioning system
tc	Thermal collector
ts	Thermal system
thp	Thermal heat pump
u	Useful
v	Water vapor
w	Water

Chapter 1: Introduction

1.1. History and development of air conditioning & refrigeration technology and current challenges

The pursuit of safe and comfortable living conditions has always been one of the main goals of the human race. Development of refrigeration and air conditioning has played a vital role in fulfilling this goal. The development and industrialization of the United States, especially the Southern states, would have never been possible without year-round control of the indoor environment. Although most of the United States population experienced a conditioned environment in the mid-to-late 20th century, the history of refrigeration and air conditioning is many centuries older.

The Greek historian Xenophon in his “Memorabilia” records some of the teachings of the Greek philosopher Socrates (470-399 BC) regarding correct orientation of dwellings to maintain houses cool in the summer and warm in winter [1]. Central heating was pioneered by the Romans using double floors through whose cavity the fumes of a fire were passed. Also, Romans were the first to use window glazing. There is also some evidence that the Chinese, Indians, Jews, and Persians understood air conditioning concepts centuries earlier, but the first documented public demonstration of refrigeration phenomenon was given in 1756 by Mr. William Cullen, a Professor of Chemistry and Medicine at the University of Edinburgh [2] .

Mr. Cullen used a pump to create a partial vacuum over a container of diethyl ether, which then boiled, absorbing heat from the surroundings. This created a small amount of ice, but the process found no commercial application. The first attempt at building an air conditioner was made by Dr. John Gorrie, an American physician, scientist, inventor, and humanitarian. During his practice in Apalachicola, Florida in the 1830s, Dr. Gorrie created an open air-cycle refrigeration machine that essentially blew air over a bucket of ice for cooling hospital rooms of patients suffering from malaria and yellow fever. Although Gorrie is considered by many as the father of air-conditioning, the list of pioneers also includes A. Muhl (who held the first patent for cooling residences--in this case with ether compression and expansion), A. R. Wolf (1859-1909; who provided comfort air conditioning to more than 100 buildings, including the Waldorf Astoria, Carnegie Hall, and St. Patrick's cathedral), and William H. Carrier.

The first system similar to the modern air conditioner units was developed in 1902 by an American engineer Willis H. Carrier (1876-1950), who not only provided the first psychrometric chart, but also set new trends in product development and marketing to control humidity inside a lithographic plant in Brooklyn, New York [3]. Controlling the humidity in printing companies and textile mills was the start of managing the inside environment. Interestingly, an early textbook on air conditioning [4] restricted air-conditioning to the process of air humidification. The

concept has broadened considerably and is now understood to be the process of controlling temperature and humidity inside a conditioned space. After the invention by Carrier, air conditioners began to bloom. They first hit industrial buildings such as printing plants, textile mills, pharmaceutical manufacturers, and hospitals. However, during the first wave of their installation, Carrier's air conditioner units were large, expensive, and dangerous due to the toxic ammonia that was used as the coolant. In 1922, Carrier had two breakthroughs - he replaced the ammonia with the benign coolant dielene and added a central compressor to reduce the size of the unit. After World War II, window unit air conditioners appeared, with sales escalating from 74,000 in 1948 to over one million in 1953 [5].

During the period of about 1950 to 1970 when the modern HVAC industry was rapidly developing, the cost of electricity was very low and the concepts such as global warming and ozone depletion were relatively esoteric. Hence, very little consideration was given to alternative modes of air conditioning. The emphasis on alternative forms of air conditioning is gaining strength due to the two most important challenges facing conventional systems of air conditioning related to environmental and energy.

1.1.1. Environmental effects

The modern air conditioning machines are affecting the environment primarily in two ways. The first is due to the emissions of

chlorofluorocarbons (CFCs) and hydrochlorofluorocarbons (HCFCs) used as refrigerants in these machines. Rowland and Molina [6] posited that chlorine atoms in CFCs and HFCs are causing the breakdown of the ozone layer in the stratosphere which shields the earth from cancer-causing ultraviolet-B solar radiation. By 1985, scientists saw a drastic thinning of the ozone layer over Antarctica, an annual phenomenon dubbed the "ozone hole." Recognizing these dangers, on September 16, 1987, world leaders from 24 nations signed the *Montreal Protocol* [7]. Since then, new scientific proofs of the urgency of ozone damage have led all 196 members of the United Nations to ratify the treaty. The production of CFCs is already phased-out and the phasing-out of less active HCFCs is expected to be complete by 2030.

The second environmental concern due to conventional air conditioning is its impact on global warming. Most of the commonly used refrigerants in Vapor Compression Refrigeration (VCR) machines have very high Global Warming Potential (GWP). For example, HFC-134 a, one of the most widely used refrigerant blends, has GWP equivalent to 1320 times of CO_2. Besides releasing greenhouse gases directly into the atmosphere through leaks, equipment maintenance, and retirements, most of the electricity generated to run these machines also comes from the burning of fossil fuels (a significant source of CO_2 emission). Greenhouse gases are widely believed to contribute to an increase in the observed average temperature of the earth's atmosphere [8], resulting in

higher cooling demand and therefore creating a positive feedback loop. Selection of natural refrigerants which are ozone friendly and have lower GWP in air-conditioning and refrigeration systems would significantly benefit goals for environmental progress.

1.1.2. Energy crisis and peak load

The conventional refrigeration cycles are primarily driven by electricity. The International Institute of Refrigeration has estimated that approximately 15% of all the electricity produced in the world is employed for refrigeration and air conditioning processes, and the energy consumption for air conditioning systems has recently been estimated as 45% of the entire residential and commercial buildings energy consumption [9]. In addition to the increasing energy consumption, the major issue facing most of the electric utilities in the Southwestern United States is the summer peak load which is causing severe stress on electricity generation and transmission & distribution systems. Utility companies in all the 12 states located in the western United States are experiencing an increasing number of peak load days during the summer time resulting in more frequent blackouts and higher cost of electricity [10, 11]. In a report prepared by Kema-Xenergy [12] on residential and commercial sector peak load energy consumption in California, central air-conditioning is found to contribute nearly 45% of the peak energy demand. Historically, policymakers and utility regulators have considered energy efficiency (EE) as the least cost strategy to help meet resource adequacy and transmission

expansion needs. Recently, state and federal policymakers and utility regulators have broadened the scope of evaluation and planning by integrating EE programs focused on achieving energy savings with programs that focus on other program objectives such as reducing dependency on fossil fuels (by Renewable Energy mandates), reducing the need for investments in generating capacity (by demand response program), and investing in technologies that help to mitigate climate change [13].

Solar powered air-conditioning is one of the most promising ways to address both environmental and energy issues as discussed above. Since most of a building's heat load is due to absorbed solar radiation, the time of day with maximum incident solar radiation would correspond roughly to the time of maximum demand. Moreover, the efficiency of solar collectors increases with increasing insolation and increasing ambient temperature resulting in higher energy collection per unit area in the summer. Additionally, solar refrigeration devices are of significance to meet the needs for cooling requirements and medical or food preservation in remote areas. Using solar powered cooling system will reduce the fossil fuel burning by reducing the required electricity generation hence reducing greenhouse gases in the atmosphere. Finally, solar thermal systems can use refrigerants which are ozone friendly as well as have zero or very small GWP.

1.2. Solar powered air conditioning systems

Several solar refrigeration and air conditioning systems have been investigated by researchers throughout the world [14, 15, 16, 17, 18, 19, 20]. These systems can be classified primarily into two different categories e.g. solar electric and solar thermal. The following section provides a brief discussion on both solar electric and solar thermal refrigeration systems.

1.2.1. Solar electric air conditioning

A solar electric system consists mainly of photovoltaic panels and an electrical air conditioning device. There are several kinds of solar electric air conditioning systems researched to-date, such as photovoltaic-powered vapor compression, thermoelectric, and Stirling refrigerator [21]. Each of these systems has their advantages and disadvantages but the photovoltaic vapor compression is probably the most widely used air conditioning system. The vapor compression refrigeration cycle requires electricity to the compressor which is provided by the solar photovoltaic (PV) panels. A schematic diagram of a solar PV vapor compression system is shown in Figure 1.1. PV panels generate electrical power by converting solar radiation into direct current electricity using semiconductors. The manufacturing of solar cells has seen a tremendous growth in recent times due to the growing demand of renewable energy. Materials presently used for solar cells include mono-crystalline silicon, poly-crystalline silicon, amorphous silicon, cadmium telluride, etc. Silicon remains the most commonly used solar cell material.

The efficiency and cost of solar cells vary widely depending on the material and the manufacturing methods from which they are made. The efficiency of a solar panel is defined as the ratio of power output to the direct solar irradiation per unit area. Solar panel efficiency can be as low as 9.5% for amorphous silicon technology to as high as 24.7% for mono-crystalline silicon technology [22]. The biggest advantage of using solar panels for air conditioning is the matured technology and high overall efficiency when combined with a conventional vapor compression system.

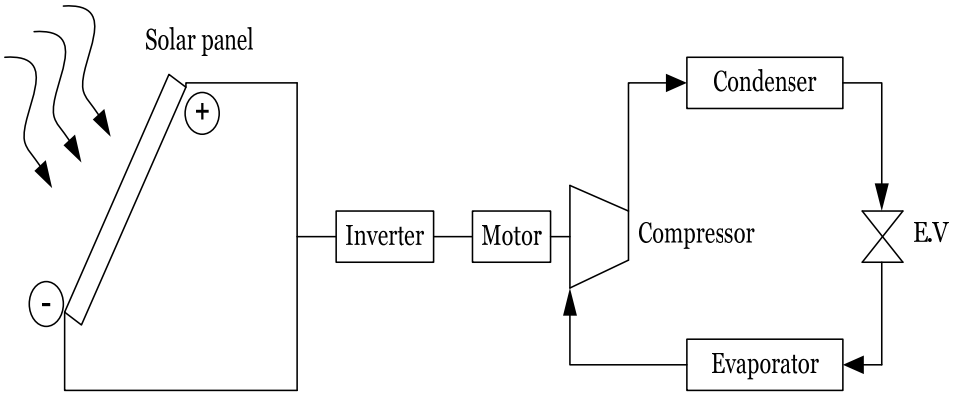

Figure 1.1. Schematic diagram of a solar photovoltaic vapor compression system

Several solar electric cooling systems were designed for autonomous operation and packaged in standard containers [23]. The cooling Coefficient of Performance (COP) of the vapor compression machines in those systems ranged from 1.1 to 3.3 for different evaporator temperatures between −5 and 15 °C and condenser temperatures between 45 and 61 °C. Mono-crystalline PV modules and variable-speed compressors were used with batteries or generators as a backup.

1.2.2. Solar thermal air conditioning

Solar thermal systems use solar heat rather than solar electricity to produce cooling effect. Primarily two types of solar thermal systems have been investigated; sorption systems and thermal-mechanical systems (Rankine and Stirling engines). However, for the residential scale, the only practical choice is the sorption system due to extremely high temperatures required to power thermo-mechanical systems. Many solar-powered (or heat-activated) sorption systems have been researched and demonstrated in recent years, including absorption, adsorption, and desiccant [9, 24, 25, 26].

1.2.2.1. Absorption system

Most of the thermally driven cooling systems today are based on absorption chillers. A schematic diagram of the absorption system is shown in Figure 1.2. In an absorption system (closed-cycle), the refrigerant is evaporated from a less volatile absorbent, the vapor is condensed in a water- or air-cooled condenser, and the resulting liquid is passed through an expansion valve to the evaporator of the unit. The refrigerant from the evaporator flows into the absorber, where it is reabsorbed in the absorbent and pumped back to the generator. In the generator, refrigerant is evaporated from the liquid solution by supplying heat from a heat source. The absorber-generator-pump combination works as a thermal compressor and hence eliminates the need for an electric compressor. Electrical energy consumed by the liquid pump is a

tiny fraction of the energy consumed by an electric compressor due to the difference in the specific density of vapor and liquid medium. Single-effect absorption systems have only one heating level of the working fluid (dilute solution). Double-effect absorption systems have two stages of vapor generation to separate the refrigerant from the absorbent and triple-effect have three stages. The heat transfer in double and triple effect system occurs at a higher temperature compared to the single-effect system.

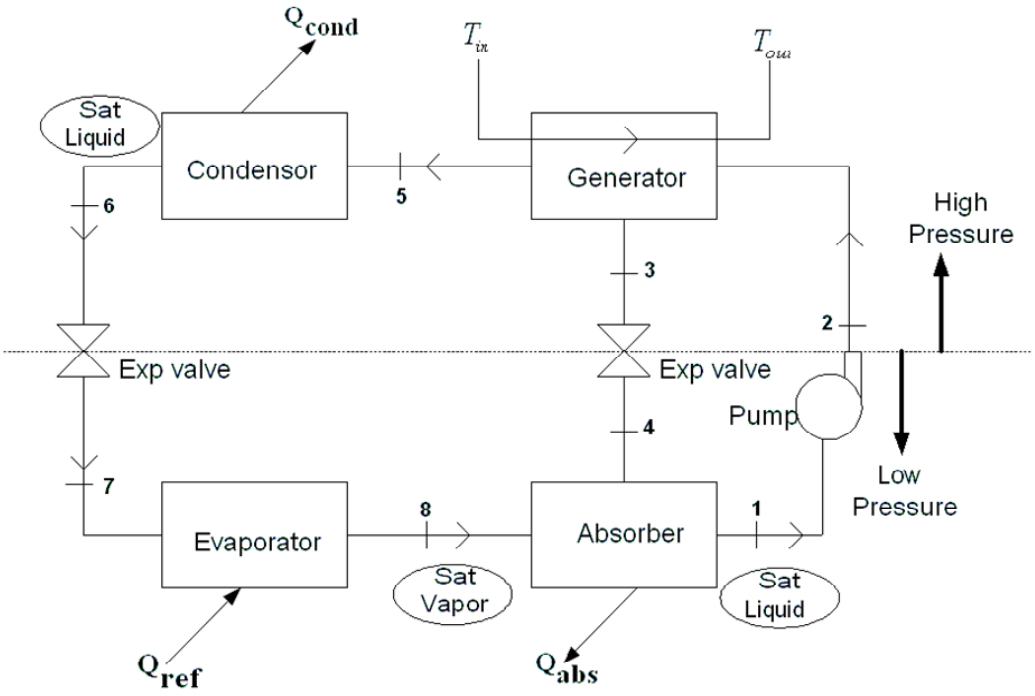

Figure 1.2. Schematic diagram of the basic absorption cooling system

Today absorption chillers are mainly installed if a heat source such as waste heat, district heat or heat from co-generation plants is readily available in the facility. Two types of absorbent-refrigerant pairs are

commonly used; water-ammonia and lithium bromide (LiBr)-water. Absorption systems have the following drawbacks for small-scale residential cooling application:

1. The driving temperature (heat source temperature) is relatively high compared to adsorption and desiccant systems. The single-effect system requires temperature range 80 – 100 ^{o}C; the double-effect between 100 – 160 ^{o}C; and triple-effect above 160 ^{o}C [27]. Since, most of the residential systems are expected to employ either flat-plate or evacuated tube solar collectors due to the higher cost of concentrated collectors, using double or triple-effect systems is not feasible. In fact single-effect systems may also remain inoperable for most of the year due to lower-than-required driving temperatures available from flat-plate/evacuated tube collectors.
2. Ammonia is toxic and harmful, so is very unsafe to use in residential systems.
3. In LiBr-water absorption chillers, usually the crystallization line for lithium bromide and water is very close to the working concentrations needed. If the solution concentration is too high or the solution temperature is reduced too low, particularly in air-cooled systems, there is a strong possibility of LiBr crystallization resulting in machine failure [28].

1.2.2.2. Desiccant system

Open-cycle sorption cooling is more commonly called *desiccant cooling* because a sorbent is used to dehumidify air. A thermally driven desiccant system is based on a combination of evaporative cooling with air dehumidification by a desiccant, i.e., a hygroscopic material. Either liquid or solid materials can be employed for this purpose. The standard cycle which is mostly applied today uses rotating desiccant wheels, equipped either with silica gel or lithium-chloride as sorption material [29]. A schematic diagram of the desiccant cooling system is shown in Figure 1.3.

A desiccant cooling system comprises principally three components, namely the regeneration heat source, the dehumidifier (desiccant material), and the cooling unit. However, the possible configurations and/or the composition of each of the three components can vary largely according to the nature of the desiccant employed [29]. For solid desiccant systems, the desiccant dehumidifier is generally a slowly rotating desiccant wheel or a periodically regenerated adsorbent bed. The cooling unit can be the evaporator of a conventional air conditioner, an evaporative cooler or a cold coil. The role of the cooling unit is the handling of the sensible load while the desiccant removes the latent load. A heat exchanger is generally used to pre cool the dry and warm air stream before its further cooling by an evaporative cooler or a cold coil. The heat exchanger together with the evaporator cooler or the cold coil constitutes the cooling unit [30]. The regeneration heat source

supplies the thermal energy necessary for driving out the moisture that the desiccant had taken up during the sorption phase. Because a thermal energy source is required, a variety of possible energy sources can be utilized. Those include solar energy, waste heat, and natural gas heating, and the possibility of energy recovery within the system.

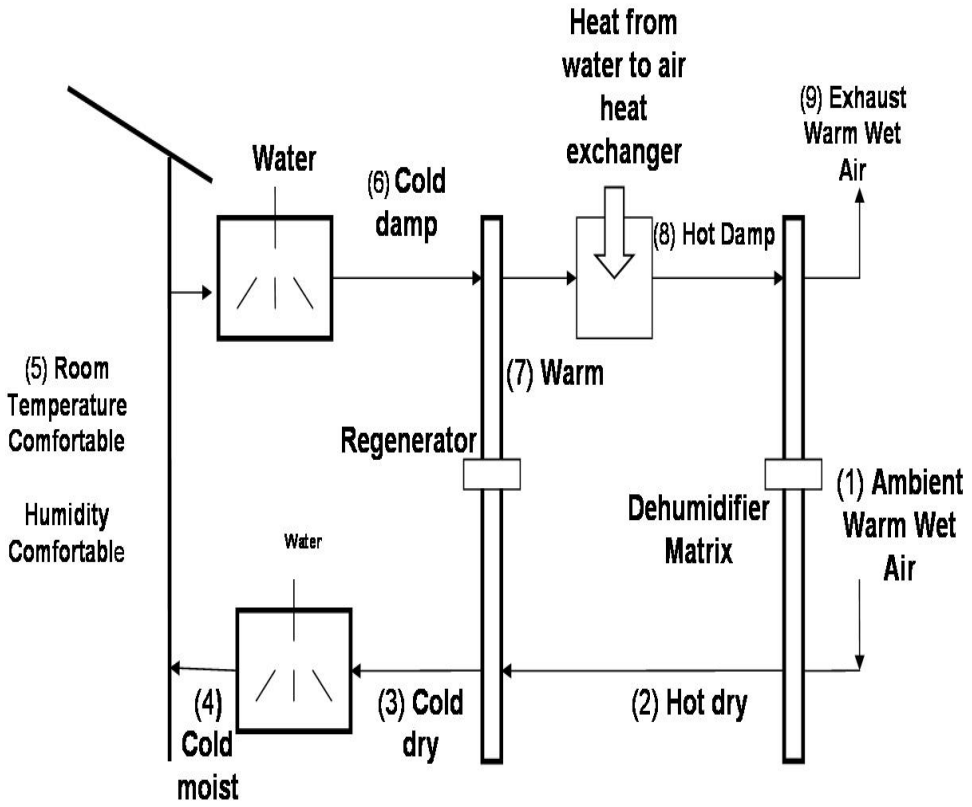

Figure 1.3. Schematic diagram of the basic desiccant cooling system

Desiccant air cooling systems have a drawback in that they cannot cool supply air below 20 °C (≈70 °F) at peak design temperatures, particularly in hot and humid conditions, therefore to maintain a design space temperature of 24 °C (≈75 °F) a relatively high volume of supply air is required. Hence desiccant air systems are relatively bulkier and bigger

in size and are also not suitable where cooling space does not need a large percentage of ventilation air [31] and has a limited space availability.

1.2.2.3. Adsorption system

Adsorption air conditioning system (closed-cycle) utilizes the phenomenon of physical adsorption between the refrigerant and a solid adsorbent. A schematic diagram of the adsorption cooling system is shown in Figure 1.4. The refrigerant vapor exiting from the evaporator is adsorbed by the adsorbent in a vessel called “adsorber.” When heat is supplied to the adsorber, the refrigerant vapor is released increasing the pressure inside the adsorber. Once the pressure inside the adsorber exceeds the condenser pressure, refrigerant vapor flows in to the condenser and is condensed. Between the condenser and evaporator, the process described above in the absorber section repeats. Typically, two or more adsorber vessels are used to make this process pseudo-continuous. The adsorption process is described in more detail in chapter 2.

Adsorption systems do not possess any of the disadvantages of the absorption and desiccant systems. They can operate with as low a driving temperature as 50 ^{o}C [27, 32], are free from crystallization because they do not use liquids for sorption of refrigerant, and are less bulky than the desiccant systems. Another major advantage of an adsorption system is that it uses environmentally benign substances such as water, methanol etc. as refrigerants. But, adsorption systems also suffer from issues such as low COP (less than 0.5 compared to about 0.8 for single-effect LiBr

system) [27], low thermal conductivity of adsorbents, and high ratio of non-adsorbent ("dead") to adsorbent ("live") thermal mass [33]. Still, low driving temperature adsorption systems remains the most attractive choice to replace conventional systems particularly for residential applications.

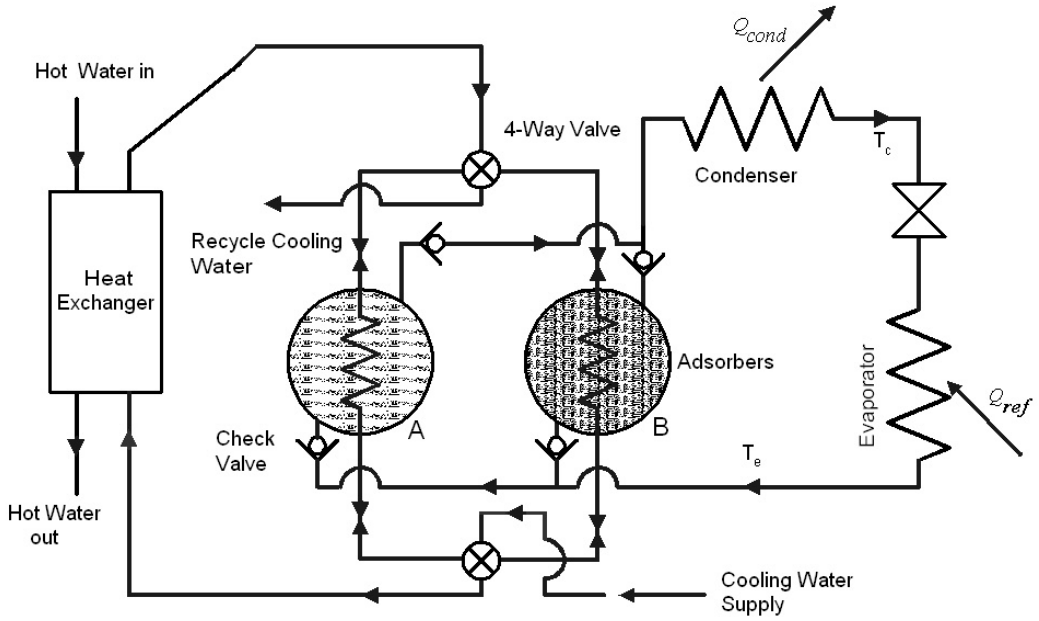

Figure 1.4. Schematic diagram of the basic adsorption cooling system

1.3. Research objectives

Each of the solar-powered air conditioning systems discussed in the above section has its advantages and disadvantages. The differences lie in the state of technical maturity, specific cost, and their respective field of application and dissemination. As a consequence, there is astonishingly little common knowledge and regrettably little synergy between the researchers of each individual field. Despite a large potential market, existing solar air conditioning systems are not competitive with

conventional vapor compression air conditioning systems primarily because of their high initial costs. However, researchers agree that solar thermal systems can provide a better alternative to vapor compression systems in the future if fossil-fuel prices continue to rise, summer peak load situation deteriorate, and addressing environmental issues becomes a priority. Solar adsorption systems seem to be one such alternative to replace conventional vapor compression systems. However, questions remain regarding the viability of adsorption systems at the small-scale and their comparison with other solar-powered cooling technologies including solar electric. The specific objectives addressed in this dissertation are as follows:

1. Investigate the thermal performance (both refrigeration capacity and the COP) of a adsorption cooling system and compare its performance with similar heat-activated technologies such as absorption and desiccant system.
2. Evaluate possible adsorbent-refrigerant pairs and chose a pair that is environmentally friendly and have favorable characteristics for a residential-scale adsorption system?
3. Demonstrate the cooling effect using a bench-scale adsorption cooling system prototype and investigate its performance.
4. Evaluate the thermal performance and economics of various solar cooling technologies for a typical single-family house in

Phoenix, AZ, and determine the optimum combination of solar collector and storage size for each system.

This work focuses on small-scale adsorption cooling systems and their relative performance with competitive solar technologies. A general introduction has already been given above in Chapter 1. The overview of adsorption process and standard adsorption cooling systems is provided in Chapter 2. A detailed discussion of mathematical modeling of adsorption cooling system is presented in Chapter 3. It also includes quantitative and qualitative comparison of various low-temperature, heat-activated cooling systems. The selection of adsorbent-refrigerant pair, prototype development, and experimental results are presented in Chapter 4. The thermal and economic comparison of solar PV, LiBr-H_2O absorption, and Silica gel-water absorption systems for a typical residential house in Phoenix, AZ is presented in Chapter 5. The details regarding the hourly load calculations, mathematical modeling, is also presented, as are the effects of collector and storage size and their optimum values. Finally, a summary and suggested future works are proposed in Chapter 6.

Chapter 2: Adsorption cooling system

The following section describes some of the important terms associated with the adsorption cooling system.

2.1. Adsorption phenomenon

Any adsorption process requires a porous solid medium (the adsorbent) and liquid/gas molecules (the adsorbate) to occupy the micropore volume. The adsorption is a consequence of the cohesive forces including electrostatic forces and hydrogen bonding at the surface of the adsorbent which attracts the molecules of the adsorbate [34]. The forces of attraction emanating from a solid may be of two main kinds, physical and chemical, and they give rise to physical (or “van der Waals”) adsorption or ‘physisorption’ and chemical adsorption or ‘chemisorption’, respectively. Molecules that are physically adsorbed to a solid can be released (desorbed) by applying heat as shown in Figure 2.1; therefore the process is reversible. The bonding forces of chemisorption are much greater than that of physisorption hence more heat is required to desorb the molecules. In addition to that, chemical bonding leads to changes in the chemical form of the adsorbed compounds and hence is irreversible. For this particular reason, physisorption is involved in most thermal systems which are cyclic in nature [25].

2.2. Heat of adsorption

Adsorption is an exothermic process accompanied by evolution of heat, commonly referred as ‘isosteric heat of adsorption’. This is the ratio

of the infinitesimal change in the adsorbate enthalpy to the infinitesimal change in the amount adsorbed. The quantity of heat release depends primarily upon the magnitude of the van der Waals force between the adsorbent and adsorbate, and the latent heat of the adsorbate. The heat of adsorption is usually 30-100% higher than the heat of condensation of the adsorbate [25]. In general, adsorption is stronger than condensation to the liquid phase. Hence, if a fresh adsorbent and adsorbate in liquid form coexist separately in a closed vessel, transport of adsorbate from the liquid phase to the adsorbent occurs in the form of vapor. The liquid temperature becomes lower while the adsorbent temperature rises. Air-conditioning and refrigeration utilize this phenomenon to obtain a cooling effect [35].

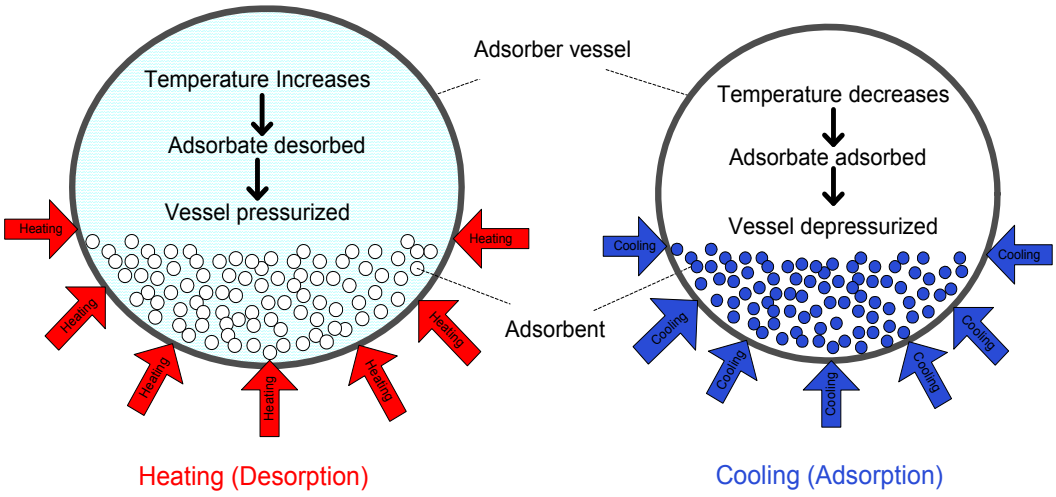

Figure 2.1. Adsorption and desorption processes

2.3. Adsorption equilibrium

The amount of gas or vapor adsorbed when equilibrium is established at a given temperature and pressure is a function of the nature

of the adsorbent and adsorbate. This includes on one hand the physical structure of the adsorbent (the surface area, the size, shape and distribution of pores) and its chemical constitution, and on the other, the physical and chemical properties of the adsorbate. Adsorption is usually described through isotherms, that is, the amount of adsorbate on the adsorbent as a function of its pressure (if gas) or concentration (if liquid) at constant temperature. Intensive investigation of the adsorption on real solids has led to the development of a large number of empirical isotherm equations. Primarily, two main classes of the overall adsorption isotherms exist:

- Equations reducible to the Langmuir isotherm
- Isotherms generated by the exponential isotherm equation

The Langmuir isotherms can be expressed as [36]:

$$q = q^{\infty}\left(\frac{bP}{1+bP}\right) \tag{2.1}$$

where q is the amount adsorbed, q^{∞} the limiting amount adsorbed, P is the pressure, and parameter b is the affinity constant or Langmuir constant. Langmuir constant is a measure of how strong an adsorbate molecule is attracted onto a surface.

Numerous well-knows empirical isotherms (Langmuir-Freundlich, generalized Freundlich, Tóth etc.) are based on Eq. (2.1). The exponential isotherm has the following form [36]:

$$q = q^{\infty} \exp\left\{ -\sum B_j \left[k_B T \ln\left(\frac{p_a}{p} \right) \right]^j \right\} \tag{2.2}$$

where B_j are temperature-independent coefficients, k_B is the Boltzmann constant, and p_a is the parameter connected with minimum adsorption energy.

Numerous well-knows empirical isotherms (classical Freundlich, Dubinin-Radushkevich, Dubinin-Astakhov, Freundlich-Dubinin-Radushkevich etc.) are based on Eq. (2.2).

2.4. Adsorbent and adsorbate

The selection of a proper adsorbent and adsorbate (referred to as the refrigerant in cooling systems) pair for an adsorption cooling system is a complex process and depends on several factors. There are several working pairs to choose from like silica gel/water, activated carbon/ water, activated carbon/ ammonia, zeolite/ water etc. [37]. The selected adsorbent must have following characteristics:

- Higher adsorption and desorption capacity (increases cooling density)
- Higher thermal conductivity (reduces the cycle time)
- Lower specific heat capacity (reduces the cycle time)
- Chemical compatibility with the chosen refrigerant
- Low cost and widely available

The selected adsorbate (refrigerant) must have most of the following desirable thermodynamic and heat transfer properties:

- Molecular dimensions should be small enough to allow easy adsorption
- High thermal conductivity and good thermal stability
- Low viscosity, low specific heat and high latent heat per unit volume
- Non-toxic, non-inflammable, non-corrosive and chemically stable
- Low saturation pressure (slightly above atmospheric) at normal operating temperatures

2.5. Basic adsorption cycle

The basic adsorption cooling system consists of an evaporator, a condenser, an expansion valve and two vessels (filled with adsorbent) shown as A and B in Figure 1.4, which switch their roles during the cycle. At any point in time, one of these vessels is being heated, while the other is being cooled. The vessel being heated generates high-pressure refrigerant (adsorbate) vapor, which subsequently increases the pressure inside it. When the pressure reaches the saturation vapor pressure of the refrigerant in the condenser, the valve between the heated adsorbent vessel and the condenser is opened and the desorbed vapor is released to the condenser, condensed to high-pressure saturated liquid, and then passed across a thermostatic expansion device to lower its pressure and temperature.

Meanwhile, the second adsorbent vessel, which is being cooled, reaches a pressure lower than the saturation vapor pressure of the refrigerant in the evaporator resulting in a flow of refrigerant vapor from the evaporator to this adsorbent vessel. The flow of refrigerant between the condenser and the evaporator is similar to the conventional vapor compression refrigeration cycle.

2.6. Literature review of adsorption cooling

Several air conditioning and refrigeration applications have been studied theoretically and experimentally using various adsorbent and adsorbate pairs. Due to the large number of articles published on adsorption systems, only major breakthrough developments are described in the following section.

The field of adsorption cooling started as a historical curiosity, had a brief period of commercial success, disappeared for 60 years and is now undergoing a renaissance. The first commercial products were in the early years of the 20th century. Plank and Kuprianoff [38] described a practical adsorption system which used methanol as adsorbate and active carbon as adsorbent and was powered by heat from fossil–fuel combustion. In 1929, Hulse [39] and Miller [40] designed an adsorption system for air-conditioning system of railway carriages. They used silica gel-sulpher dioxide pair with a propane-fired heat source to cool the carriages to -12 ^{o}C. However, following the advent of cheap reliable compressors and

electric motors, this and other types of “sorption” systems went out of favor.

The first modern revival of interest was in the late 1970s when Meunier [41] began work on pairs suitable for use as solar refrigerators. In 1988, Tchernev [42] designed, constructed and performance tested a closed-cycle regenerative zeolite-water heat pump of 0.5 - 2 tons (1 ton = 12,000 Btu/hr = 3.51 kW) capacity and found a seasonal cooling Coefficient of Performance (COP) of 0.15. Saha et el. [43] in 1995 conducted an experimental and numerical study on a 10 kW silica-gel water adsorption system and obtained a COP between 0.21-0.48. He also found that each adsorption/desorption cycle required nearly 3-13 min, and the heat recovery cycle about 30 s. In 1996, Miles and Shelton [44] designed and tested a solid-sorption heat-pump system using a thermal wave regeneration concept and activated carbon/ammonia pair and found a significant increase in the COP theoretically, but could not reproduce the results experimentally. A quasi-continuous heat and mass recovery operation was developed and tested by Wang [45] in 2000. He found that the heat recovery operation between two adsorption beds will increase the COP by about 25% if compared with a one-adsorber basic cycle system. For the activated carbon/methanol pair, he found a theoretical COP between 0.6-0.8 and an experimental COP between 0.32-0.4. In 2001, Saha et al. [32] proposed a two-stage non-regenerative adsorption chiller design and experimental prototype using silica gel-water as the adsorbent

refrigerant pair. The main advantage of the two-stage adsorption chiller was its ability to utilize low-temperature solar/waste heat (40 – 75 ^{o}C) as the driving heat source in combination with a coolant at 30 ^{o}C. With a 55 ^{o}C driving source in combination with a heat sink at 30 ^{o}C, the COP and the cooling capacity of the two-stage chiller was found to be 0.36 and 3.2 kW respectively. Zhang et al. [46] proposed a combined adsorption-ejector refrigeration in 2002 and found a COP of 0.3 which was 10% higher than the adsorption system alone. In 2004, Liu et al. [47] proposed and tested a novel adsorption chiller with no refrigerant valve, thus eliminating the problem of mass transfer resistance occurring in the conventional systems when methanol or water is used as refrigerant and resulting in pressure drop during the flow of refrigerant inside the tubing. They found a COP of about 0.5 and cooling power of 9 kW for 13 ^{o}C evaporation temperature. Wang et al. [48] designed and tested a 10 kW novel silica gel-water adsorption chiller and found a COP of 0.38. This adsorption chiller used three vacuum chambers: two adsorption/desorption (or evaporation/condensation) vacuum chambers and one heat pipe working vacuum chamber as the evaporator. The operating reliability of the chiller was estimated to be greatly improved because of fewer required valves. In 2005, Sharkawy et al. [49] attempted to improve the performance of thermally powered adsorption cooling systems by selecting a new adsorbent/refrigerant pair. Their use of activated carbon fiber/ethanol pair showed that it can be used to design a compact adsorption unit. A

novel compact adsorption room air conditioner with a cooling capacity of 1 kW was designed , and two prototypes were built by Yang et al. For the first prototype, a cooling capacity of 687 W and a COP of 0.307 was obtained. For the second prototype, a cooling capacity of 790 W and a COP of 0.446 was obtained. Huangfu et al. [50] experimentally investigated an adsorption chiller for micro-scale building cooling, heating and power system application. They found that the COP is high in the operating mode of varying hot water inlet temperature with mass recovery in no heating pattern. Lambert [51] designed and analyzed a solar powered adsorption heat pump with ice storage and predicted a COP of 1.5. He suggested using helical annular finned tubes and metal wool to diffuse heat throughout the adsorber to improve the COP. A 1 kW adsorption cooling system was also demonstrated by Yang et al. at Shanghai Jiao Tong University in 2006. The prototype has a size as 500 mm width, 300 mm thickness, and 950 mm height. At the work condition of 85 ^{o}C of heating water inlet and 28 ^{o}C of cooling water inlet, a cooling capacity of 995 W and a COP of 0.477 was obtained. In 2009, Abdullah et al. [52] built and tested a novel solar thermoelectric-adsorption cooling system. Cooling was produced via the Peltier effect during the day, by means of thermoelectric elements, and through adsorption process at night. The COP values were determined using derived equations and found to be ~0.131 (adsorption) and ~0.152 (thermoelectric), respectively. Zhai et al. [53] constructed a solar adsorption cooling system in the green building of Shanghai Institute of

Building Science. The system consisted of evacuated tube solar collector arrays of area 150 m^2, two adsorption chillers with nominal cooling capacity of 8.5 kW for each and a hot water storage tank of 2.5 m^3 in volume. According to experimental results under typical weather condition of Shanghai, the average cooling capacity of the system was 15.3 kW during continuous operation for 8 h. The performance analysis showed that solar radiant intensity had a more distinct influence on the performance of solar adsorption cooling system as compared with ambient temperature. It was observed that the cooling capacity increased with the increase of solar collector area, whereas, solar collecting efficiency varied quite contrary. With the increase of water tank volume, cooling capacity decreased, while, the solar collecting efficiency increased. Additionally, it was observed that solar collecting efficiency decreased with the increase of the initial temperature of water in the tank; however, cooling capacity varied on the contrary. Banker et al. [54] developed a laboratory model of continuous flow closed-cycle thermal compression based solid sorption refrigeration unit using the activated carbon + HFC 134a adsorbent-refrigerant pair. The unit was tested with heat loads up to 5 W. The system performance was assessed through COP. The observed COP was not large because of over sizing of some of the compressor components. It was concluded that if the components are more critically sized by eliminating the solenoid valves and optimizing the mechanical design of the adsorbers, substantial improvement can be obtained. A novel composite water

sorbent “silica modified by calcium nitrate” (SWS-8L) was tested in a lab-scale adsorption chiller driven by low-temperature heat [55]. Thermodynamic cooling COP was estimated to be 0.51–0.71, with desorption temperature lower than 90 °C. SWS-8L grains were embedded inside a compact aluminum heat exchanger with high thermal efficiency. Experimental cooling COP, mass specific cooling power and volumetric specific cooling power obtained were 0.18–0.31 (cycle time 10 min), 190–389 W/kg dry sorbent and 104–212 W/m^3, respectively.

Chapter 3: Numerical simulation of the adsorption cooling system

Although extensive experimental and simulation work has been done to analyze the adsorption cooling system performance individually or to compare its performance with that of the vapor compression system, few attempts have been made to compare its quantitative and qualitative performance with other competing thermally-activated systems. The two main goals of the numerical modeling and computer simulation of the basic adsorption cooling system are 1) to conduct a parametric study to determine the effects of operating conditions on cooling output and COP and 2) to compare the relative performance of the adsorption system with two other competitive thermally-activated systems, e.g. a LiBr-H_2O absorption system, and a desiccant air system.

The potential of a two-bed silica gel-water adsorption system was evaluated by a number of researchers. Saha et. al. [56] conducted a parametric study using computer simulation to determine the effects of operating conditions on cooling output and COP. The results have been compared with experiments [43] and it was concluded that the silica-gel water adsorption cycle is well suited to low-temperature heat sources. Chua et al. [57] presented a transient model for a two-bed silica gel-water adsorption chiller and obtained very good agreement with experimental data. Wang et al. [48] predicted the performance of a novel silica-gel adsorption chiller and found it more reliable and efficient because it used fewer valves and exhibited high COP. The silica gel-water

adsorbent/adsorbate pair is selected in this analysis due to its relatively low regeneration temperature and because water has a large latent heat of vaporization.

3.1. System configuration and operation

The basic adsorption cooling system chosen for this study is shown in Figure 1.4 in Chapter 1. The Clapeyron diagram of the basic adsorption cycle is shown in Figure 3.1, depicting the variations of pressure and temperature inside the adsorber. The cycle consists of one desorption step (heating phase) and one adsorption step (cooling phase).

Desorption Step (abc):

The adsorber is heated by hot water, supplied from a solar or other system, from temperature T_{ads} to T_{gen}. The heat adsorbed by the adsorber includes the sensible heat of the adsorber material, adsorbent, and the adsorbate in addition to the heat of desorption. The pressure in the adsorber increases as the temperature of the adsorber is increased. When the pressure reaches the saturation vapor pressure of the water in the condenser, the valve between the adsorber and the condenser is opened and the desorbed vapor from the adsorber is condensed in the condenser. The condensate flows down continuously into the evaporator through the expansion valve until the temperature in the adsorber becomes T_{gen}.

Adsorption Step (cda):

The adsorber is cooled from T_{gen} to T_{ads} by cooling water. The heat released by the adsorber includes the sensible heat of the adsorber

material, adsorbent, and the adsorbate in addition to the heat of adsorption. The pressure in the adsorber decreases as the temperature of the adsorber is decreased. When the pressure reaches the saturation vapor pressure of the water in the evaporator, the valve between the adsorber and the evaporator is opened and the vapor from the evaporator is adsorbed in the adsorber until the temperature reaches T_{ads} in the adsorber.

Figure 3.2 shows the standard adsorption cycle on T-s diagram for the ideal cycle. The thermodynamic cycle consists of following seven processes:

Process 1-2: Isobaric heating of the refrigerant vapor to adsorber temperature (adsorber cooling source temperature);

Process 2-3: Isothermal adsorption of the refrigerant vapor to sub-cooled liquid;

Process 3-4: Isosteric heating of the sub-cooled liquid refrigerant to desorption temperature (adsorber heating source temperature);

Process 4-5: Isothermal heating of the liquid refrigerant to high-pressure superheated vapor;

Process 5-6: Isobaric cooling and condensation of the refrigerant vapor in the condenser to saturated liquid;

Process 6-7: Isenthalpic expansion of the liquid refrigerant in the expansion valve to liquid + vapor mixture;

Process 7-1: Isobaric evaporation of the refrigerant in the evaporator.

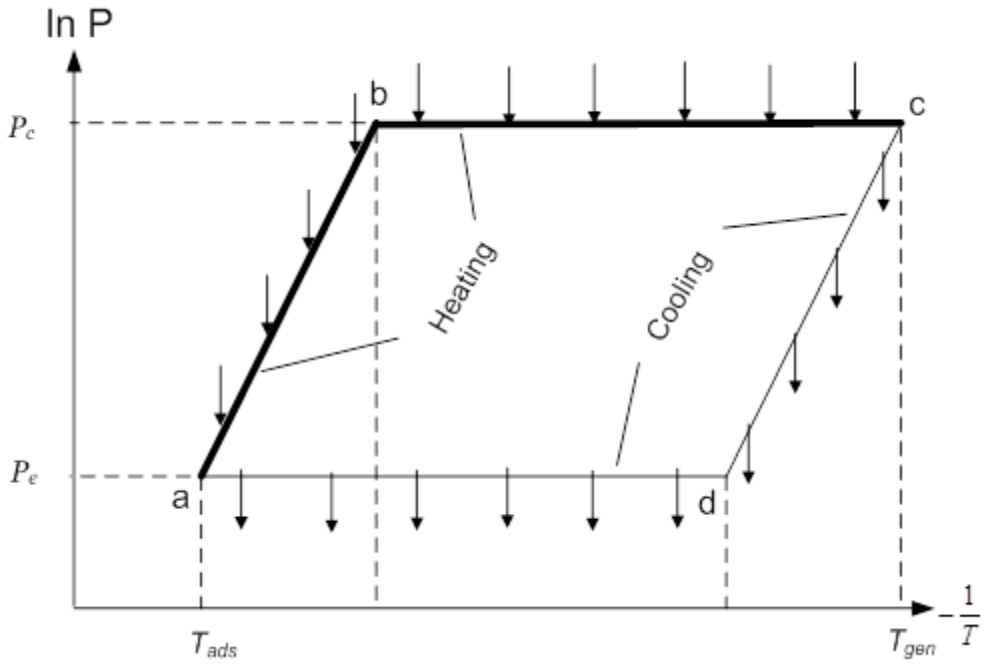

Figure 3.1. Clapeyron diagram of the adsorption cooling cycle

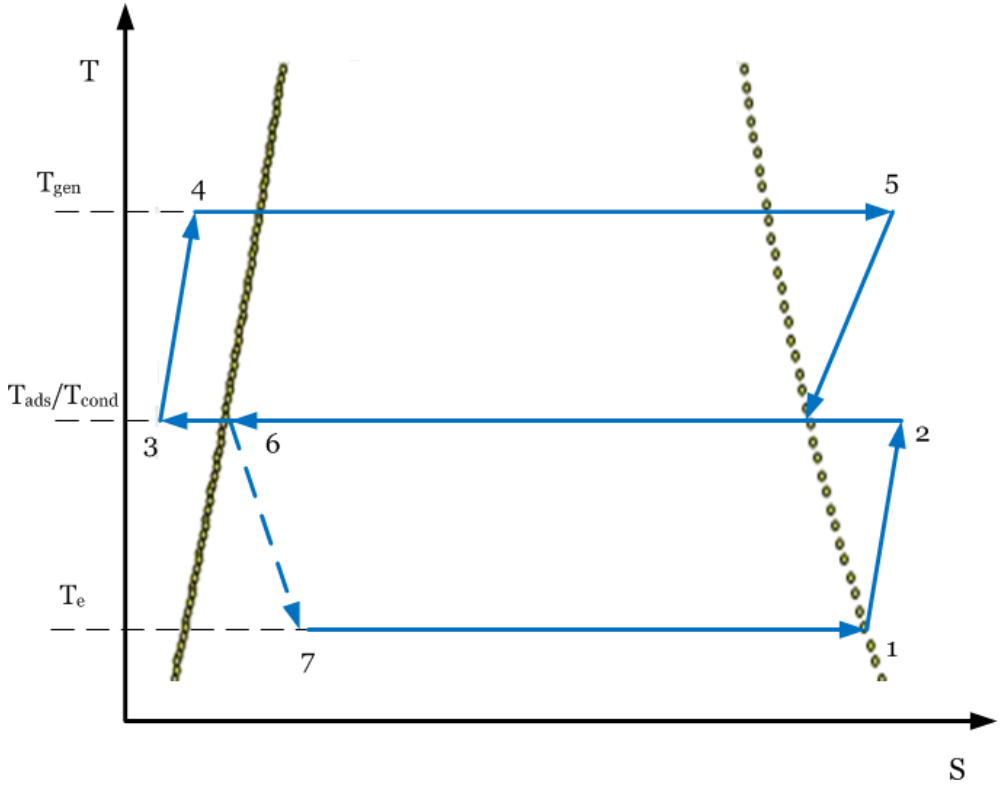

Figure 3.2. T-S diagram of a standard adsorption cooling cycle

3.2. Mathematical model

For setting up the mathematical model of the system, it is assumed that the cooling ability of the condenser is unlimited, the heat loss to the surroundings is negligible, the temperature and pressure are uniform in the adsorber, and the adsorption and desorption processes run for the same time with zero switching time.

The Freundlich equation, which assumes an equilibrium process without hysteresis and isobaric adsorption-desorption and is recommended by many investigators [58, 59], is used to model the adsorption equilibrium in the present analysis:

$$q = q^{\infty}\left(\frac{P}{P_{sat}}\right)^{\frac{1}{k}} \tag{3.1}$$

where q is the amount adsorbed, q^{∞} the limiting amount adsorbed, k a constant, P the vapor pressure within the adsorber, and P_{sat} the saturation vapor pressure at the temperature of the refrigerant. The refrigerant temperature in the vapor phase is defined by the temperature of the evaporator (during adsorption) or condenser (in desorption).

The amount adsorbed during the regeneration step is:

$$q = q^{\infty}\left(\frac{P_{sat}(T_c)}{P_{sat}(T_{ads})}\right)^{\frac{1}{k}} \tag{3.2}$$

where T_{ads} is the temperature inside the adsorber and T_c the condenser temperature. The amount adsorbed during the adsorption step is:

$$q = q^{\infty}\left(\frac{P_{sat}(T_e)}{P_{sat}(T_{ads})}\right)^{\frac{1}{k}} \tag{3.3}$$

where T_e is the evaporator temperature. The saturation pressure of the water vapor can be expressed as [60]:

$$P_{sat} = 0.001\exp(a_s + \frac{b_s}{T}) \tag{3.4}$$

where P_{sat} is in bar and T is in K. a_s and b_s are constants whose values for water are: a_s = 20.5896 and b_s = -5098.26. The heat transfer rate from the heat transfer fluid to the adsorber is expressed as:

$$\dot{Q} = \dot{m}_w C_{pw}\varepsilon\left(T_w - T_{ads}\right) \tag{3.5}$$

where $\dot{m}_w$ is the mass flow rate, C_{pw} the specific heat, and T_w the temperature of the heating or cooling water. ε is the effectiveness of the adsorber which is expressed as:

$$\varepsilon = 1 - \exp\left[-\frac{UA_{ads}}{\dot{m}_w C_{pw}}\right] \tag{3.6}$$

where U is the overall heat transfer coefficient and A_{ads} the surface area of the adsorber. The desorption heat balance is:

$$\left[M_{am}C_{am} + M_{ad}(C_{ad} + qC_{pw})\right]\frac{dT_{ads}}{dt} + M_{ad}H_{ad}\frac{dq}{dt} = \dot{Q} \tag{3.7}$$

where M_{am} and C_{am} are the mass and the specific heat of the metallic adsorber, and M_{ad} and C_{ad} the mass and the specific heat of the adsorbent.

H_{ads} is the isosteric heat of adsorption for the adsorbent. The adsorption heat balance is:

$$\left[M_{am}C_{am} + M_{ad}(C_{ad} + qC_{pw})\right]\frac{dT_{ads}}{dt} + M_{ad}(H_{ad} + C_{pv}(T_e - T_{ads})\frac{dq}{dt} = \dot{Q} \tag{3.8}$$

where C_{pv} is the specific heat of saturated water vapor at the evaporator temperature. The mass flow rate of the refrigerant flowing in the cycle can be determined as:

$$\dot{m}_{ref} = \frac{2M_{ad}(q_{conc} - q_{dil})}{t_{cycle}} \tag{3.9}$$

where q_{conc} is the adsorbed amount at the end of the adsorption step, q_{dil} the adsorbed amount at the end of the desorption step, and t_{cycle} the cycle time. A factor of *2* is used because of considering a two-adsorber system. The refrigeration capacity per cycle of the system is:

$$\dot{Q}_{ref} = \dot{m}_{ref}\left(h_v(P_e) - h_f(P_c)\right) \tag{3.10}$$

The rate of heat input per cycle can be calculated as:

$$\dot{Q}_{in} = (\dot{m}_{ref}H_{ad}) + \frac{(M_{am}C_{am} + M_{ad}(C_{ad} + q_{conc}C_{pw}))}{(t_{cycle}/2)}(T_{g1} - T_{a1}) \tag{3.11}$$

where the first term on the RHS of Eq. 3.11 is due to the heat of adsorption, and the second term is the sensible heat required to heat the adsorber material, adsorbent, and the adsorbate (water) from the temperature at the end of the adsorption process, $T_{a1,}$ to the temperature at the end of the desorption process, T_{g1}. Finally, the Coefficient of Performance (COP) can be calculated as:

$$COP = \frac{\dot{Q}_{ref}}{\dot{Q}_{in}} \tag{3.12}$$

Table 3.1 shows the list of parameters used in this adsorption cooling cycle simulation. One parameter at a time was varied to investigate its effect on the refrigeration capacity and COP while the remaining parameters were fixed at the standard operating conditions. Table 3.2 shows the values of standard operating conditions used in the simulation.

The system of differential equations (3.1) – (3.12) was solved simultaneously by numerical integration using Matlab inbuilt solver ODE 45.

3.3. Validation of the numerical solution

The numerical solution is validated by comparing the results with the experimental results obtained in reference [43] for similar size and type of system using same adsorbent-refrigerant pair. As shown in Table 3.3, the COP is about the same and refrigeration capacity in the simulation results is higher compared to experimental results due to higher heating source temperature.

Table 3.1. Physical property values used in the simulation

Parameters	Value	Unit
Specific heat of adsorber material, C_{am}	448	J kg^{-1} K^{-1}
Specific heat of adsorbent (i.e. silica gel), C_{ad}	920	J kg^{-1} K^{-1}
Specific heat of water vapor, C_{pv}	1,866	J kg^{-1} K^{-1}
Specific heat of water, C_{pw}	4,180	J kg^{-1} K^{-1}
Heat of adsorption, H_{ad}	2800	kJ kg^{-1}
Constant, k	0.79	-
Mass of adsorber material, M_{am}	20	kg
Mass of adsorbent, M_{ad}	20	kg
Surface area of adsorber, A_{ads}	3	m^2
Maximum adsorption, q^{∞}	0.355	-
Overall heat transfer coefficient of the adsorber, U	300	W m^{-2} K^{-1}

Table 3.2. Standard operating conditions used in the simulation

Parameter	Value	Unit
Mass flow rate of cooling/heating water, $\dot{m}_w$	0.4	kg s^{-1}
Temperature of cooling water, $T_{w,cool}$	27	^oC
Temperature of heating water, $T_{w,hot}$	80	^oC
Condenser Temperature, T_c	29	^oC
Evaporator Temperature,T_e	19	^oC
Cycle Time, t_{cycle}	480	s

Table 3.3. Validation of the numerical solution

	T_c (°C)	T_e (°C)	$T_{w,hot}$ (°C)	$\dot{m}_w$ (kg s^{-1})	COP	$\dot{Q}_{ref}$ (kW)
Experimental	30	12	50	0.58	0.35	1.2
Simulation	29	19	65	0.40	0.32	4.0

3.4. Cycle simulation results

Figure 3.3 shows the effect of varying heating water temperature on the refrigeration capacity of the system. Refrigeration capacity increases with the heating water inlet temperature and approaches towards a steady state. This behavior can be explained by the fact that more and more refrigerant gets desorbed in the adsorber due to the increased heat supply but eventually reaches its maximum value because of the limiting capacity of the adsorbent to hold the refrigerant. The COP initially increases and then decreases with increasing hot water temperature as shown in Figure 3.4. This is due to the fact that initially refrigeration capacity increases faster than the heat input and hence COP increases but the opposite become true after the temperature reaches about 70 °C. The Carnot COP of the adsorption cooling cycle is defined as:

$$COP_{Carnot} = \left(1 - \frac{T_c}{T_{w,hot}}\right) x \left(\frac{T_e}{T_{w,cool} - T_e}\right) \tag{3.13}$$

using simulation parameters of T_c = 29 °C (302 K), $T_{w,hot}$ = 65 °C (338 K), T_e = 19 °C (292 K), and $T_{w,cool}$ = 27 °C (300 K), the ideal COP is calculated

to be 3.89. In comparison, the calculated maximum COP from the simulation is 0.33.

Similar effects on refrigeration capacity and COP are observed by varying the heating water mass flow rate as shown in Figure 3.5 and Figure 3.6. The sole effect in this case is similar to increasing the hot water inlet temperature, as both result in providing more heat to the adsorber, therefore, the trends of the curves are also similar. Since mass of the silica gel used in the simulation is 20 kg, approximately 400 W of cooling per kg of adsorbent is achieved by the adsorption system.

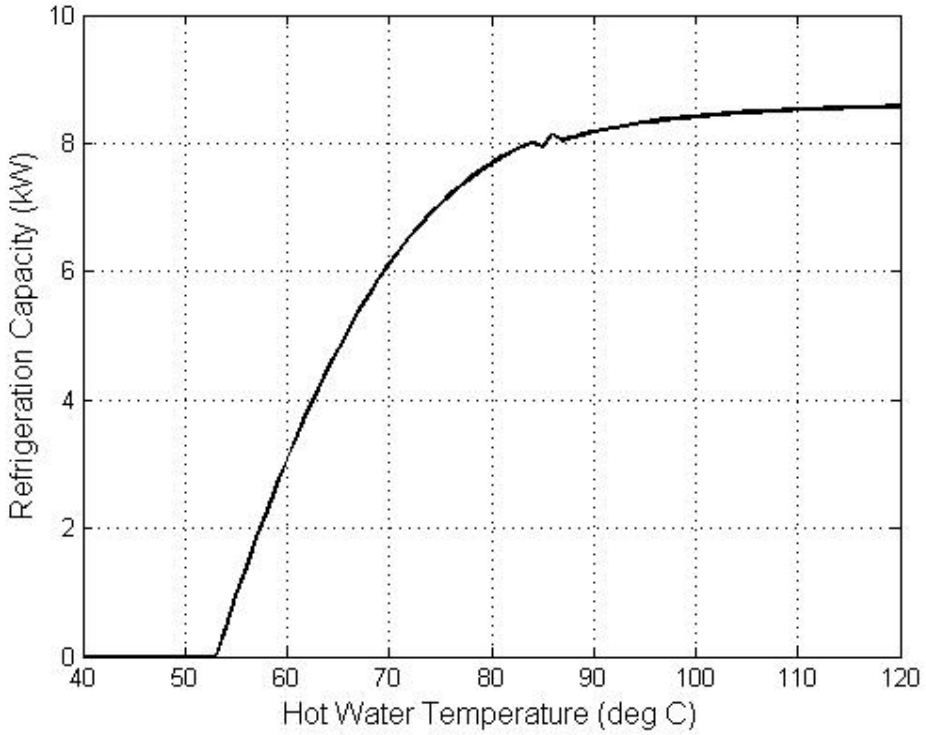

Figure 3.3. Heating water temperature effect on refrigeration capacity

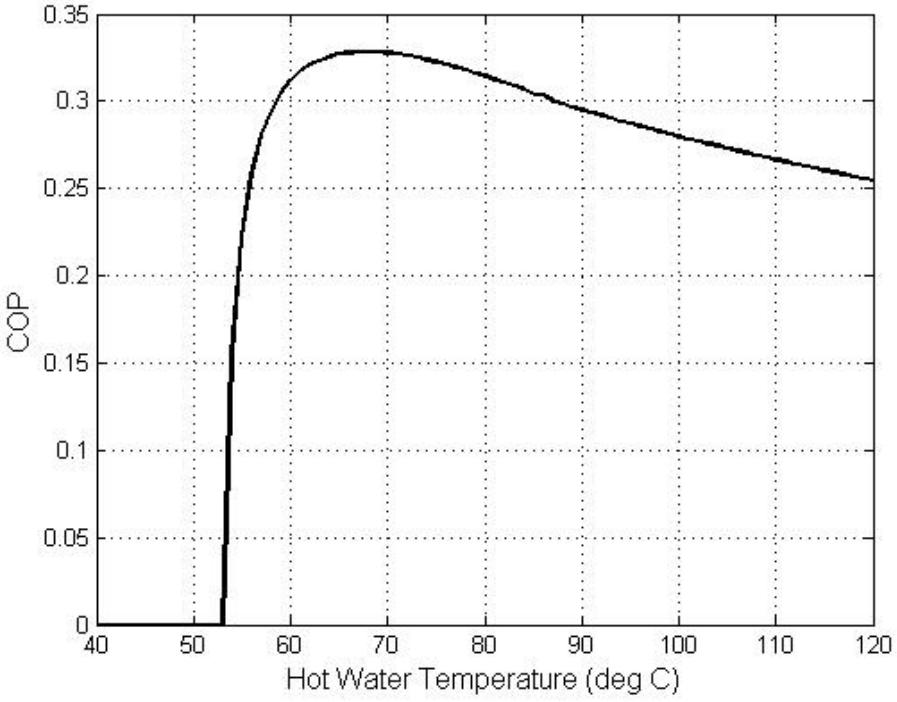

Figure 3.4. Heating water temperature effect on COP

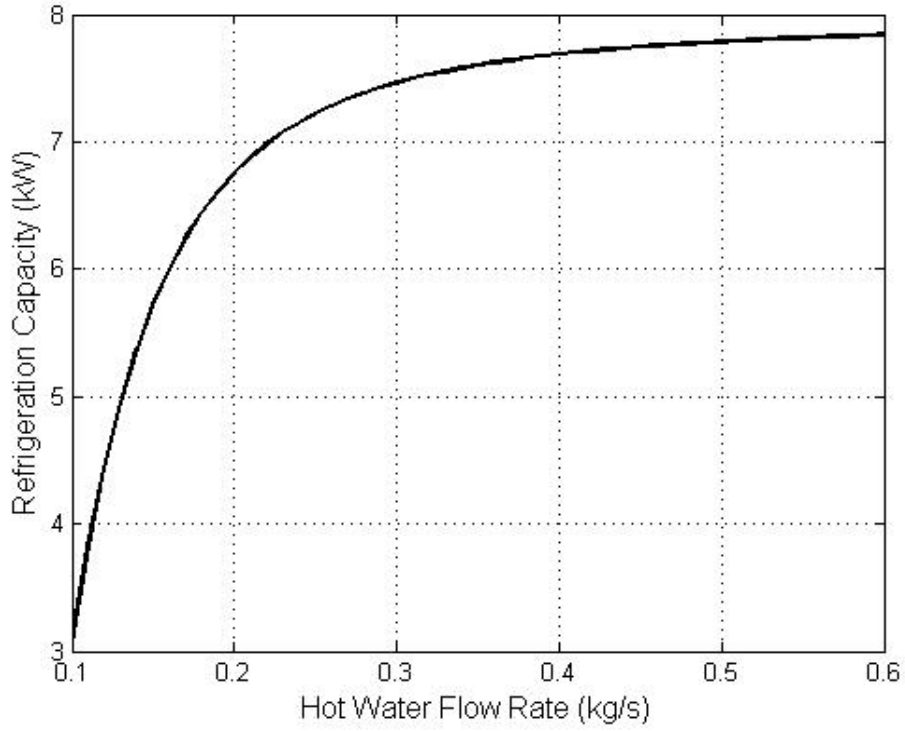

Figure 3.5. Heating water mass flow rate effect on refrigeration capacity

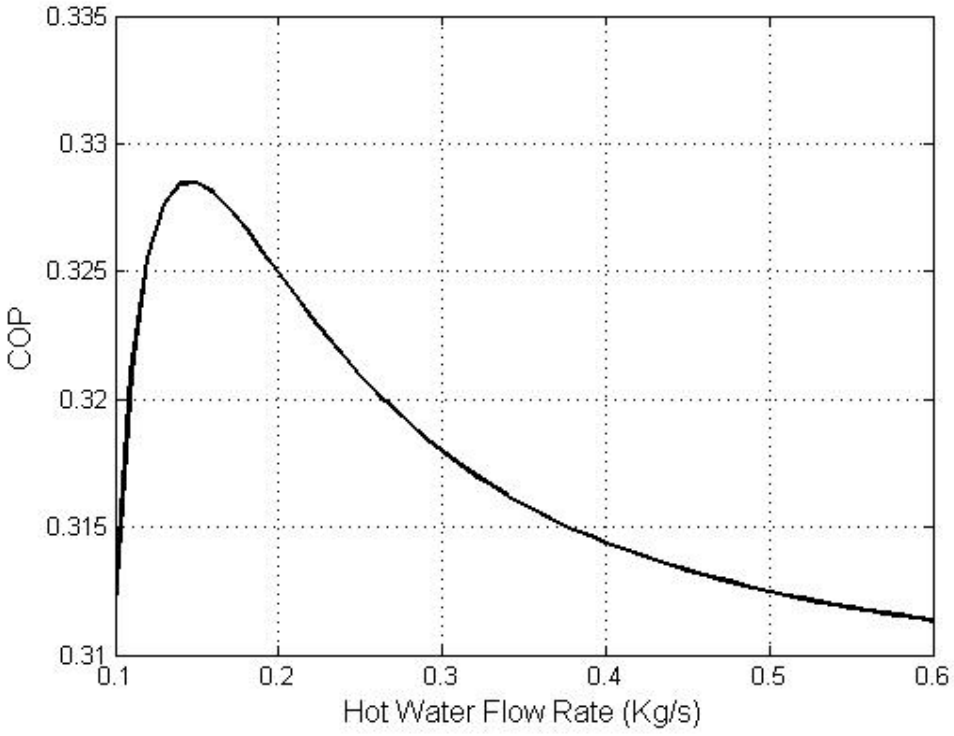

Figure 3.6. Heating water mass flow rate effect on COP

Figure 3.7 shows the effect of varying cooling water temperature on the refrigerating capacity of the system. The refrigerating capacity decreases from nearly 10 kW to 4 kW as the cooling water inlet temperature is increased from 20 to 40 ^{o}C. This tendency reflects the fact that higher adsorption temperatures result in smaller amounts of refrigerant being adsorbed and hence desorbed during each cycle. It is also clear from Figure 3.7 that a minimum regenerating temperature lift is required to produce any cooling from an adsorption system.

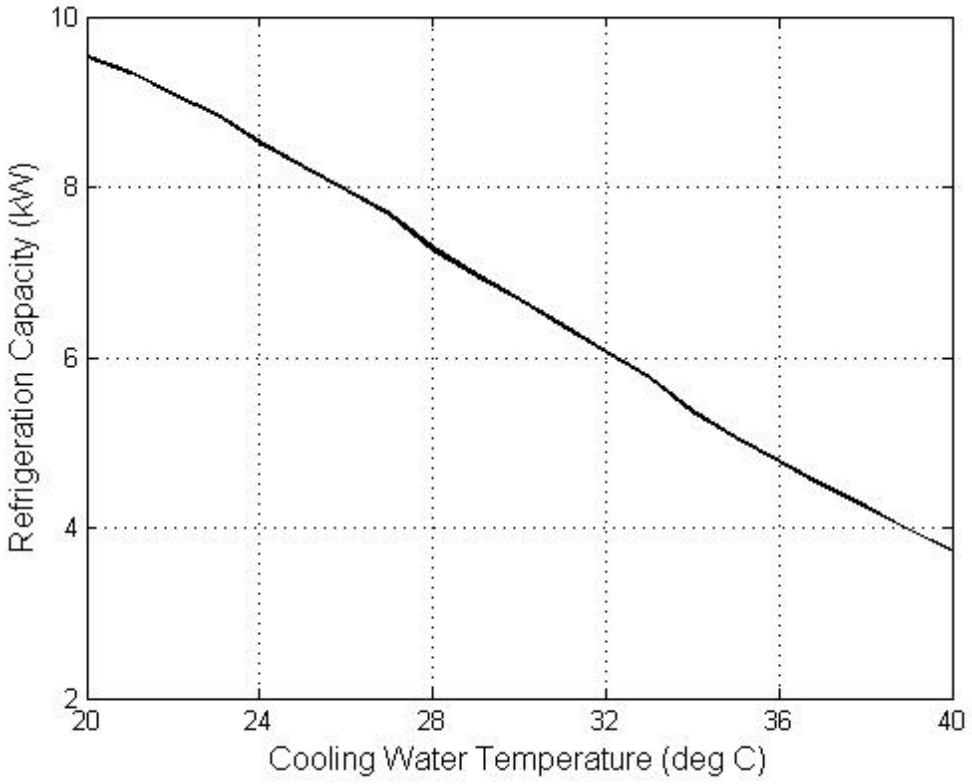

Figure 3.7. Cooling water temperature effect on refrigeration capacity

The rate of decrease in COP of the system increases with increasing cooling water temperature as can be seen in Figure 3.8. COP is affected by two opposite factors when cooling water temperature is increased; on one side the refrigerating capacity decreases, and on the other side the amount of driving heat required for sensible heating of the adsorber from adsorption to desorption temperature also decreases. The decrease in COP indicates the dominance of the first factor over the second one i.e. refrigerant capacity is very sensitive to any change in cooling water temperature. Figure 3.9 shows the effect of adsorption-desorption cycle times on the refrigeration capacity of the system. The highest cooling

capacity can be obtained near 380 s or roughly in the range between 300 and 500s. When the cycle times are shorter than 300 s, there is not enough time for adsorption and desorption to occur satisfactorily and the cooling capacity decreases. For longer cycle times, the cooling capacity decreases because adsorption and desorption tend to be relatively less intense near the later part of the cycle which results in lower refrigeration capacity. The COP monotonically increases with cycle time as shown in Figure 3.10, because of lower consumption of driving heat with longer cycles. It appears to be reaching an asymptotic value for higher cycle times than those considered in the simulation.

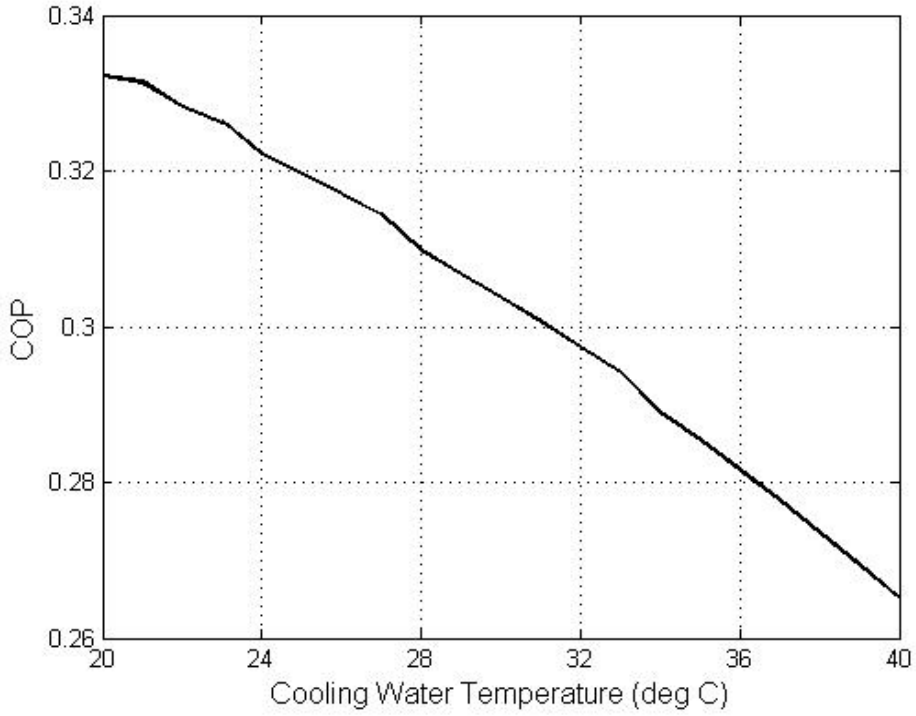

Figure 3.8. Cooling water temperature effect on COP

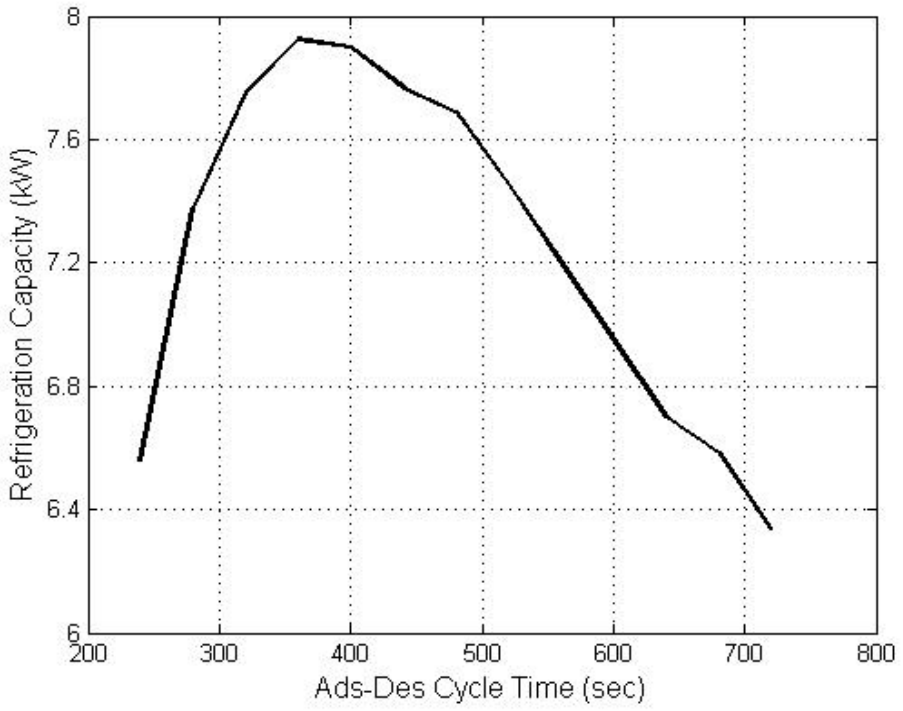

Figure 3.9. Adsorption-desorption cycle time effect on refrigeration capacity

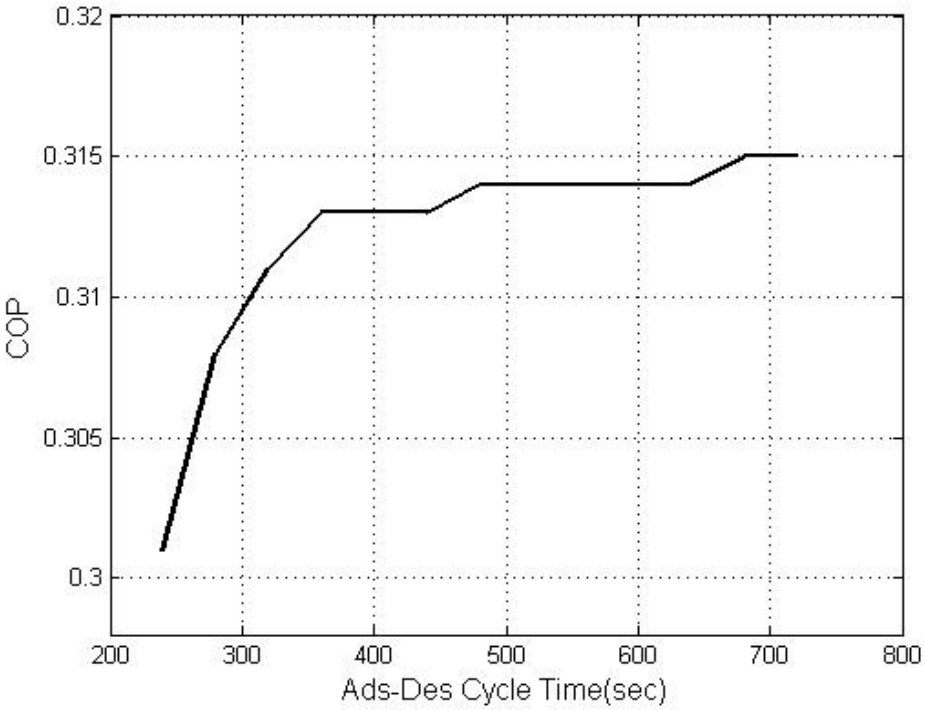

Figure 3.10. Adsorption-desorption cycle time effect on COP

3.5. Comparison with competitive technologies

In addition to the adsorption system, two other heat-activated refrigeration systems, namely absorption and desiccant air systems are considered to be the most common thermally-activated cooling systems. Each of these systems can be utilized at relatively low heat source temperatures such as achieved by flat-plate solar collectors, but it is unclear which of these systems is best suited to what range of heat source temperature. In the current study all these three systems are compared quantitatively based on their relative thermal performance, and also qualitatively based on the size, maturity of technology, safe operation, etc. For the comparison with silica gel-water adsorption cooling system, a LiBr-H_2O absorption cooling system and a silica-gel based desiccant air cooling system is selected due to their use of water and silica gel respectively. In order to provide a fair comparison between the fundamentally different systems, a *UA* (overall heat transfer coefficient multiplied by the heat transfer area) value of 1.0 kW/ ^oC is considered for the heat exchanger that transfers heat from the supplied hot water. Furthermore, to compare systems of similar size, the mass of silica gel in the adsorption and the desiccant systems, and the mass of LiBr-H_2O solution in the absorption system were specified such that each system provides the same amount of refrigeration (8.0 kW) at a source temperature of 90 ^oC.

3.5.1. Quantitative comparison

Figure 3.11 shows the effect of the hot water temperature on the refrigeration capacity. All curves intersect at 90 °C because we fixed the mass of silica gel and LiBr-H_2O solution such that the same refrigeration capacity is delivered by all systems at that temperature. It can be observed from Figure 3.11 that both the adsorption and absorption systems provide equal refrigeration capacity for a hot water temperature range of 70-120 °C, but the adsorption system is the only system to deliver cooling at temperatures below 65 °C. The desiccant system works better at higher temperatures, but its cooling capacity declines linearly with decreasing temperatures, and the system is nonfunctional at low temperatures.

Figure 3.12 shows the effect of hot water temperature on the COP for the three systems. Increasing the heating water temperature does not make the desiccant air cooling system more or less efficient. This is because for optimal performance, a desiccant system has a maximum regenerating air temperature requirement. The absorption and desiccant systems provide better COP at low temperatures, but the COP's of the three systems converge at higher temperatures. The COP of the adsorption system first increases, reaches a maximum value, and then deceases with increasing hot water temperature, because of the size limitation in utilizing the thermal heat of high-temperature hot water. The high COP's achieved by the absorption system are somewhat misleading, as they have more to

do with the flow rates occurring in the hot-water heat exchanger than with a more efficient utilization of thermal energy.

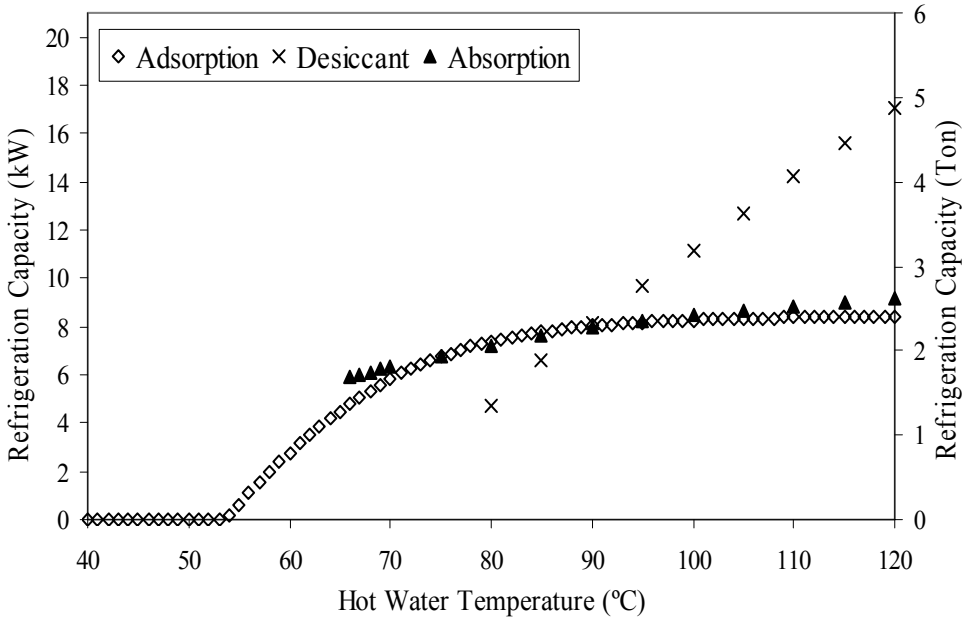

Figure 3.11. Effect of the hot water temperature on the refrigeration capacity for three types of heat-activated refrigeration systems

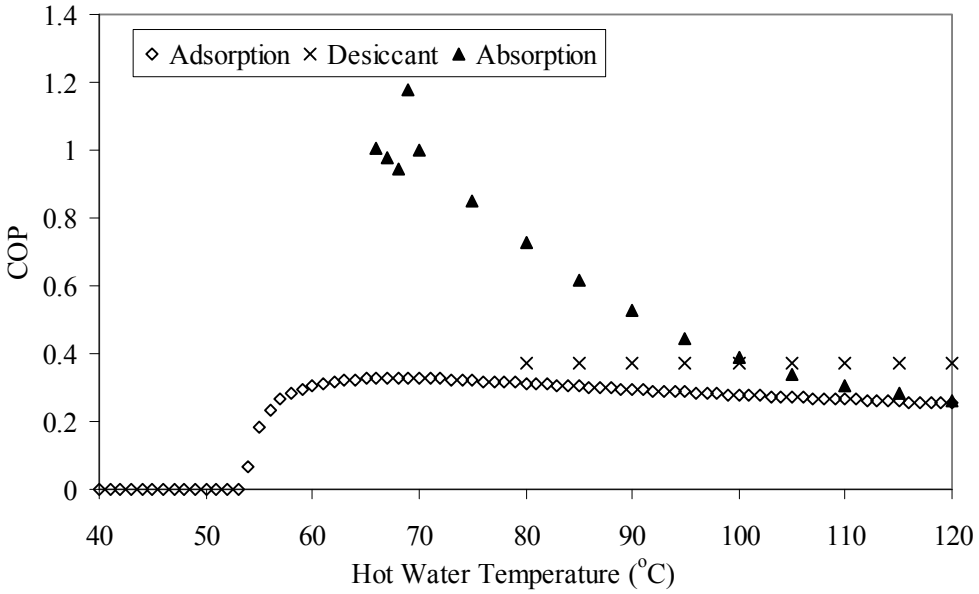

Figure 3.12. Effect of the hot water temperature on the COP for three types of heat-activated refrigeration systems

3.5.2. Qualitative comparison

Table 3.4 shows a qualitative comparison between the three cooling technologies based on available cooling sizes, maturity of technology, and safety of operation. LiBr-H_2O absorption systems are commercially available between 5 - 2500 tons unit sizes but sales are limited to greater than 100 tons units. Desiccant systems are available between 2 - 5 tons sizes and adsorption systems are in larger than 20 tons. Adsorption systems were invented before the conventional vapor compression systems and significant research is done to improve its performance. It is widely believed to attain its maturity in terms of technology and further improvement in thermal performance is implausible. Desiccant air system technology is also in similar position. Adsorption systems are still in research stage and technology can further improved. LiBr (uninhibited or corrosion inhibited solutions) poses environmental health and safety impacts. Most notably, LiBr is a known carcinogen which contains Chromium (VI) which is associated with cancer in humans. Adsorption and desiccant systems are environmental friendly.

Table 3.4. Qualitative comparison of heat-activated cooling technologies

Cooling Technology	LiBr-H_2O Absorption	Desiccant	Silica-gel Water Adsorption
Available system size	Commercial units available 5 – 2,500 tons, but sales are mostly in > 100 tons [61]	140 to 280 cmm [61]	>20 tons
Specific cooling power [62]	High	Low	Low
Maturity of technology	Mature technology for large-size, gas-powered systems	Mature technology	Commercial gas-fired systems available but mostly in development stage
Safety of operation	LiBr is hazardous for health and hard to dispose	Safe	Safe

Chapter 4: Experimental investigation

The inefficiencies in the heat and mass transfer process inside the adsorber is recognized by many investigators as the main reason for low COP and specific cooling power (SCP) of adsorption cooling systems. Research groups around the globe [42, 51, 63, 64, 65] agree that two most important parameters that must be improved in order to enhance the system performance are (a) the ratio of adsorbent ("live") mass to non-adsorbent ("dead") thermal mass, and (b) the overall heat transfer rate, both of them must be maximized [51]. This requires increasing regeneration and simultaneously minimizing non-adsorbent mass that is heated and cooled with the adsorbent, but contributes nothing to the cooling effect, thereby lowering COP and SCP.

Another important criterion in the design of an adsorption cooling system is the selection of the adsorbent and adsorbate combination. In the previous investigations, the following adsorbent and adsorbate combinations have been used most commonly:

- Silica-gel/water [32, 47, 66]
- Silica-gel/methanol [67]
- Zeolite/ water[42, 46, 68]
- Activated carbon/ammonia [44]
- Activated carbon/methanol [69, 70]

In this chapter, first the experimental set-up has been described followed by the criterion utilized to select the adsorbent and adsorbate combination. Finally, experimental results are presented.

4.1. Experimental set-up

The experimental system as shown in Figure 4.1 includes two adsorber vessels, an air-cooled condenser, a tube-in-tube water-cooled evaporator, a metering valve, and a secondary circuit to measure the refrigeration effect. Two resistance heaters were installed between the two adsorbers in order to simulate the solar or waste heat. Two pressure transducers (PT), five thermocouples (TC), and a mass flow meter was installed at various locations in the system for data collection. All temperature, pressure, and mass flow rate data were recorded into a computer through a data acquisition system from National Instruments. Figure 4.2 shows a photograph of the experimental system.

4.1.1. System components

Two adsorber vessels were used to make the adsorption cycle pseudo-continuous, where adsorption and desorption occur concurrently in different vessels. Both vessels were cylindrical in shape and about 0.11-m in diameter and 0.19-m tall as shown in Figure 4.3. The cases of these units were made from deep drawn stainless steel shells, which were reformed to create a dome shape at the ends. The open ends were formed to permit the two shells to slip together and be brazed. The reformed ends were drilled in a polar array to facilitate installation, removal and

replacement of the adsorbent, and the holes were formed into nipples to receive the stainless steel tubes, which were brazed in place.

Total fifty six (56) stainless steel tubes of 4.0-mm diameter and 0.0508-mm wall thickness were inserted in each vessel to transfer the hot and cold air require for heating and cooling the adsorber vessels. The use of extremely thin steel tubes allowed decreasing the thermal resistance between the adsorbent and the heating/cooling medium as well as decreasing the dead thermal mass of the system. Additionally, due to the small diameter and high number of tubes, the distance from tubes to any point in the adsorber has been decreased, therefore, reducing the effective thermal conductance distance.

The center of one end of each adsorber was equipped with a ½ inch NPT fitting to connect to the rest of the system. Each adsorber was connected to a tee fitting that had two gate valves. The upper valves discharge to the air cooled condenser for which an automotive transmission cooler is employed. Total surface area of the condenser was 0.11 m^2. The lower valves permit flow to leave the evaporator and reenter the adsorber. The condenser discharge was routed through a sight glass and a micrometer-metering valve, which served as an adjustable expansion valve into the evaporator. The evaporator was a flat concentric coil of aluminum tubing with total tube length of 13 ft and surface area of 0.12 m^2. The chilled water was supplied over the evaporator tubes through vinyl tubing using a counter flow tube-in-tube heat exchanger. The chilled

water inlet temperature was maintained constant at about 23.5 ^{o}C using a constant temperature bath.

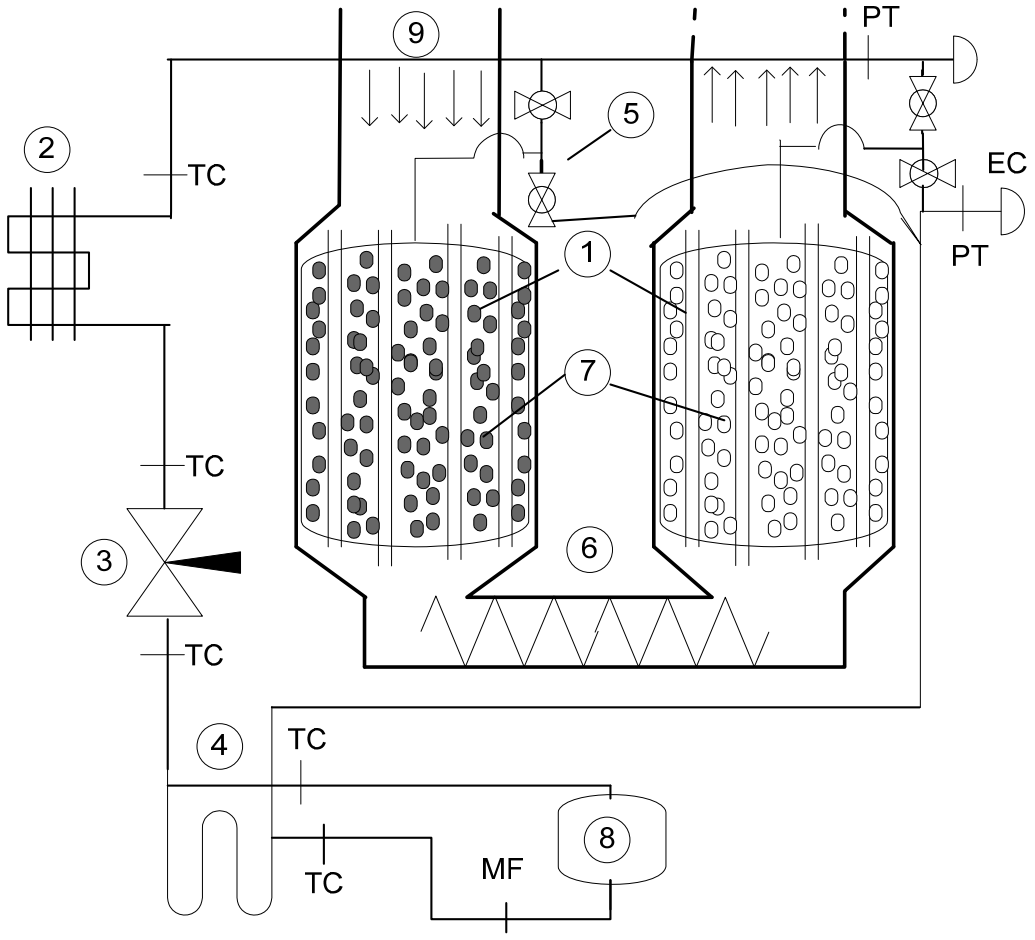

Figure 4.1. Schematic diagram of the adsorption cooling system

1. Adsorbers (two), 2. Condenser, 3. Expansion valve, 4.Evaporator, 5. Control valves (four), 6. Resistance heater, 7. Activated carbon pellets (Aadsorbent), 8. Constant temperature bath, 9. Air supply, TC: Thermocouple (five), PT: Pressure transducer (two), MF: Mass flow meter, EC: End cap (two).

The adsorbers were housed in a pair of air ducts that route air over the adsorbers and are connected at the bottom by a duct fitted with two (2) resistive heating elements of 750 Watt capacity. Because the same air

passes through the adsorber being cooled and the adsorber being heated, it eliminated the need of a separate fluid circuit for the cooling and heating of the adsorbers. This also resulted in some heat recovery by extracting heat from the vessel finishing desorption (and starting adsorption) to the vessel finishing adsorption and must be heated up to desorption temperature.

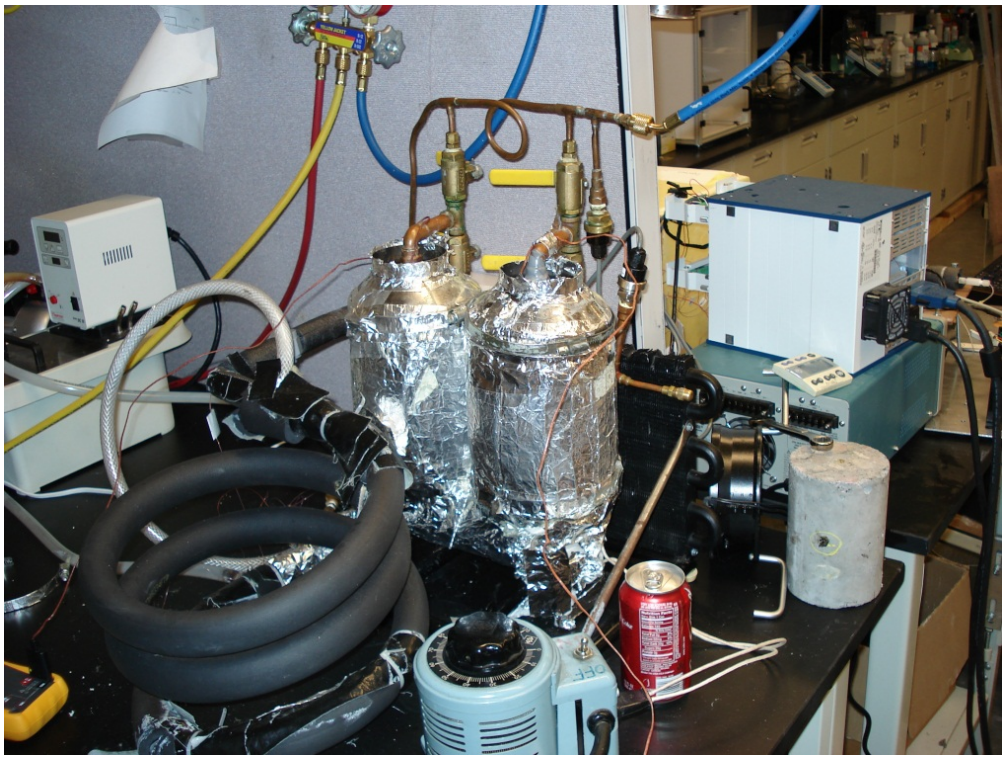

Figure 4.2. Adsorption system experimental set-up

Figure 4.3. Top view of the adsorber vessel

4.1.2. Selection of the adsorbent-adsorbate pair

Selection of the adsorbent-refrigerant pair depends on many factors but primarily depend on the designed temperature range of the cooling system. Based on the ASHRAE recommendations, an evaporator temperature of 13 ^{o}C is chosen and since the experiment is conducted inside the lab, a condenser temperature of 35 ^{o}C is selected. Table 4.1 illustrates relevant thermophysical and other properties of various refrigerants and adsorbents pairs at 1 atmospheric pressure and 25 ^{o}C temperature.

Regeneration temperature of zeolite is higher (> 140 ^{o}C) compared to activated carbon (AC) and silica gel [25, 42], therefore it is decided to

not consider it for this experiment. Water is not chosen here as the refrigerant because of its low vapor pressure, requires large pipe sizes and also can lead to air leaking into the system. Ammonia is rejected due to its toxic nature while methanol also has a negative saturation pressure (vacuum) at evaporator temperature, therefore not considered. Although affinity of butane and activated carbon is not very high but due to its above atmospheric saturation pressure in the chosen temperature range and favorable latent heat per unit volume, butane and activated carbon was chosen as the working pair. The Ozone Depletion Potential (ODP) of butane is zero and the Global Warming Potential (GWP) is about 4.0 making it an environmentally friendly refrigerant. This combination of pair was never tried earlier in an adsorption cooling system, so its novelty also provided an added incentive.

Table 4.1. Properties of selected adsorbent-refrigerant pairs at 1 atm and 25 ^{o}C

Adsorbent-refrigerant pair	Adsorbent thermal conductivity (W m^{-1} K^{-1})	Adsorbent specific heat (kJ m^{-3} K)	Latent heat at 1 atm (P_{evap}) (kJ m^{-3})	Driving temperature (^{o}C)	Saturation pressure (bar)		Adsorptivity (kg/kg) x 100
					@ 13 ^{o}C	@ 35 ^{o}C	
Silica gel-Water	0.025	112	1,747 (1,912)	50 ~ 100	0.015	0.056	35.5
Silica gel-Methanol	0.025	112	165 (177)	85 ~ 95	0.122	0.325	50
Zeolite (13 X)-Water	0.70	1,391	1,747 (1,912)	140 ~ 300	0.015	0.056	30
Activated carbon-Ammonia	0.20	420	493 (437)	120 ~ 300	6.832	13.50	29
Activated carbon-Methanol	0.20	420	165 (177)	90 ~ 150	0.122	0.325	45
Activated carbon-n-Butane	0.20	420	1,640 (1,593)	60 ~120 [71]	**1.640**	**3.266**	25.9

Butane cartridges were purchased from local grocery store. A sample Cartridge picture is shown in Figure 4.4. About 250 g of butane was used to charge the system. Activated carbon was provided by the manufacturer “Norit Americas Inc” and a sample is shown in Figure 4.5. It was marketed with a brand name “SORBONORIT® 4”, and described as a steam activated extruded carbon with a pellet diameter of 4mm. Appendix A shows the relevant properties of “SORBONORIT® 4” published by the manufacturer . Each adsorber vessel was charged with 750 g of the activated carbon.

Figure 4.4. Butane cartridge used as refrigerant in the adsorption system

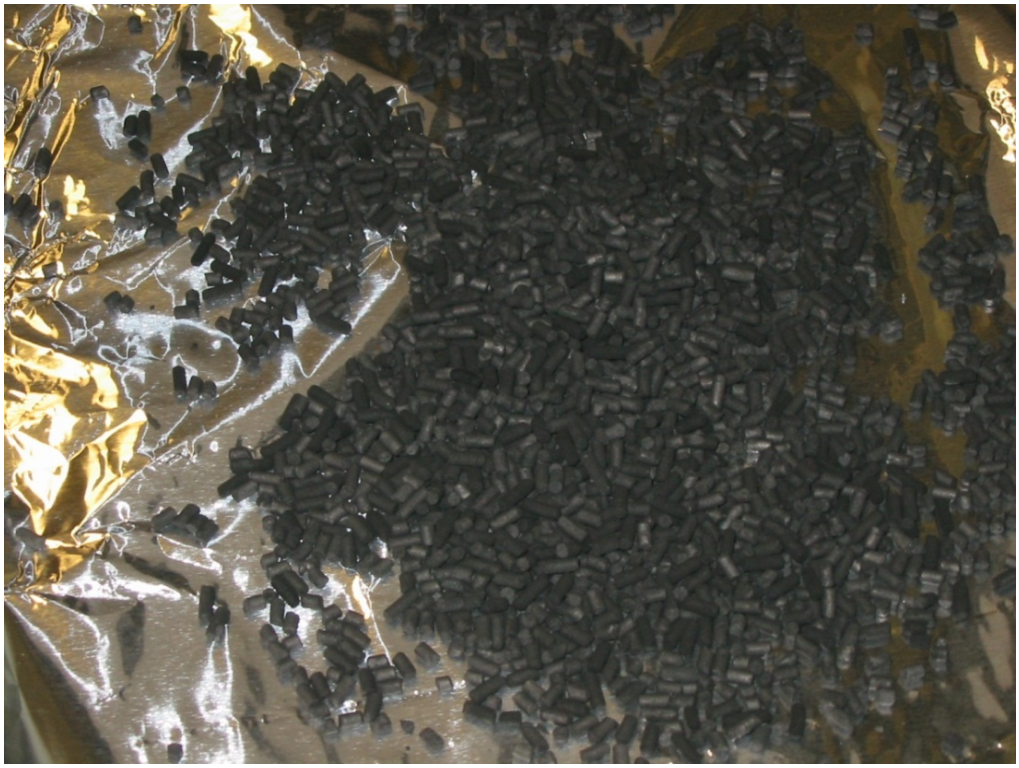

Figure 4.5. Activated carbon sample used as adsorbent in the adsorption system

4.2. Operating cycle

The cycle consists of three phases. Assume that the cycle starts when adsorber bed 1 (left bed) in Figure 4.1 is finished desorption and bed 2 (right bed) finished adsorption, and the pressure in the two adsorbers is same, because all the valves between the two has been opened allowing the pressure to equalize to take advantage of the mass recovery. After a few seconds of mass recovery, the valves connecting both adsorbers are closed. In the first phase, the heat transfer fluid, which is air, recovers heat from the initially hot bed 1, has a further heat addition by electric heaters and then proceeds to heat the initially cool bed 2. As the heating of the bed 2 proceeds, it desorbs refrigerant vapor which is driven into the condenser

and bed 1 adsorbs refrigerant vapor from the evaporator which provides cooling. Desorbed high pressure refrigerant vapor is condensed to high-pressure saturated liquid, and then passed through a metering valve to lower its pressure and temperature. This low-pressure two-phase mixture travels through the evaporator, where it flashes to vapor absorbing heat from the cooling load just like in the evaporator of a conventional vapor-compression system. At the end of phase 1, bed 1 is at evaporator pressure, P_e, and bed 2 is at condenser pressure, P_c. In the second phase, all the valves are opened between the two adsorbers to accomplish mass recovery, by allowing the pressure of the two adsorbers to equalize, which reduces the net power consumption. In the third phase, the air flow is reversed, hence the air recovers heat from the bed 2, gets heated by the electric heater and finally heats bed 1. Bed 2 adsorbs while bed 1 desorbs refrigerant vapor in this phase. At the end of phase three, bed 2 is at P_e and bed 1 is at P_c. Clapeyron diagram of the complete cycle is shown in Figure 4.6. Cycle a-b-c-d represents a conventional cycle whereas a-a'-b'-c-c'-d represents the heat and mass recovery adsorption cycle.

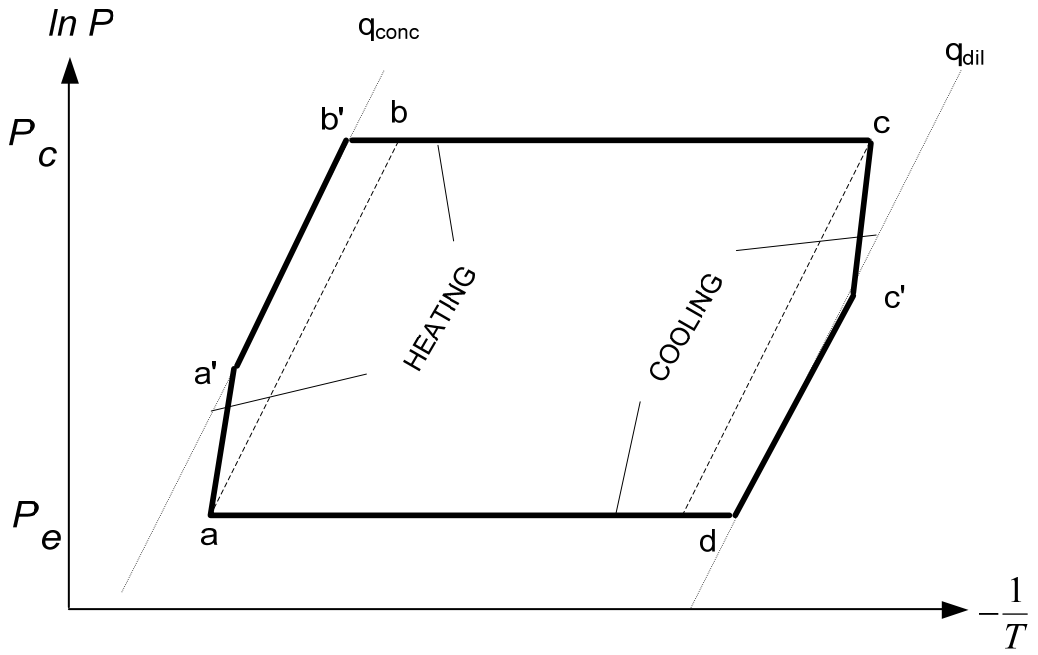

Figure 4.6. Clapeyron diagram of the heat and mass recovery adsorption cooling cycle

4.3. Test results and discussion

4.3.1. Pressure and temperature histories

Figure 4.7 shows the variations in the evaporator & condenser pressure with time. Cycle time (adsorption-desorption) for the experiment was set at 360 s. When the adsorber connected to condenser is heated, the pressure rises between the connecting tubing due to desorption of the refrigerant vapor. Simultaneously, another adsorber which was connected to the evaporator and being cooled causes drop in the evaporator pressure due to adsorption of the refrigerant vapor. At the end of half-cycle, when all the valves are opened, pressure on both sides reaches an equilibrium resulting into some mass recovery. It is clear that although a significant variation is visible in pressure variations from one cycle to another, it was

possible to obtain about 25 psig pressure difference across the expansion valve. Figure 4.8 shows the variations in the chilled water inlet and outlet temperature. As can be seen, a drop of about 2.0-3.5 ^{o}C is achievable in the chilled water temperature.

The variation in the pressure may be caused by the unsymmetrical heating and cooling of the two adsorbers and due to leaks in the adsorber vessel. We found that due to weakness in the brazed joints between heat transfer tubes and the adsorber vessel, refrigerant started to leak within few minutes of starting the experiment. When a leak appears, the whole set-up needs to be disassembled, leaks detected and fixed, and then re-assembled. Additionally, because activated carbon is a strong absorber of the water vapor, adsorber vessels used to be heated in an oven for 2-3 days and then evacuated using a vacuum pump to desorb the water vapor. All these steps used to take about 15-30 days. We have repeated this experiment many times but each time system leaks appear.

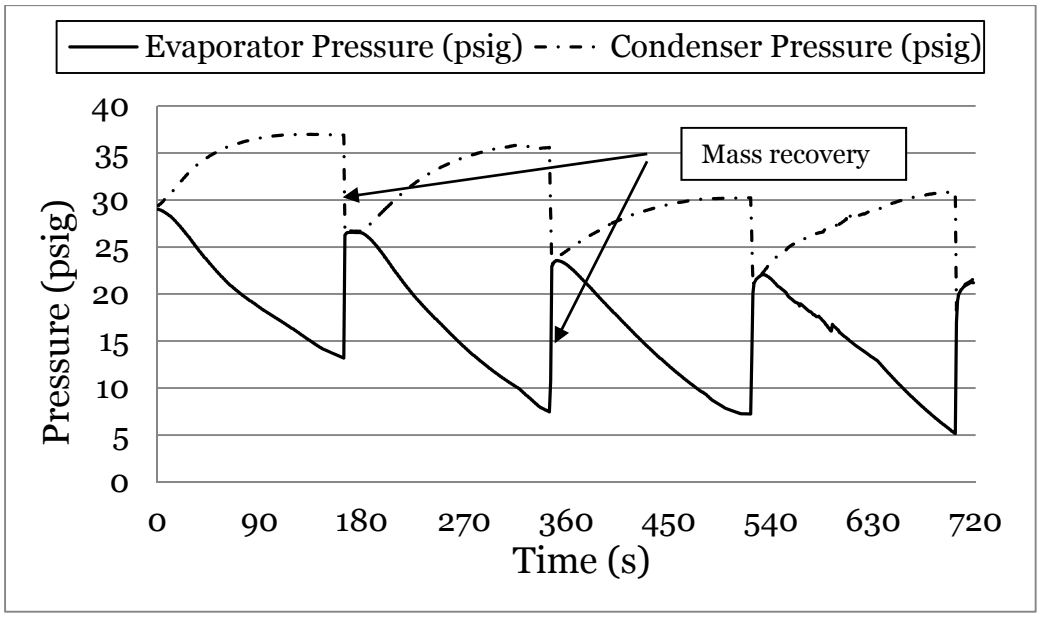

Figure 4.7. Evaporator and condenser pressure variation

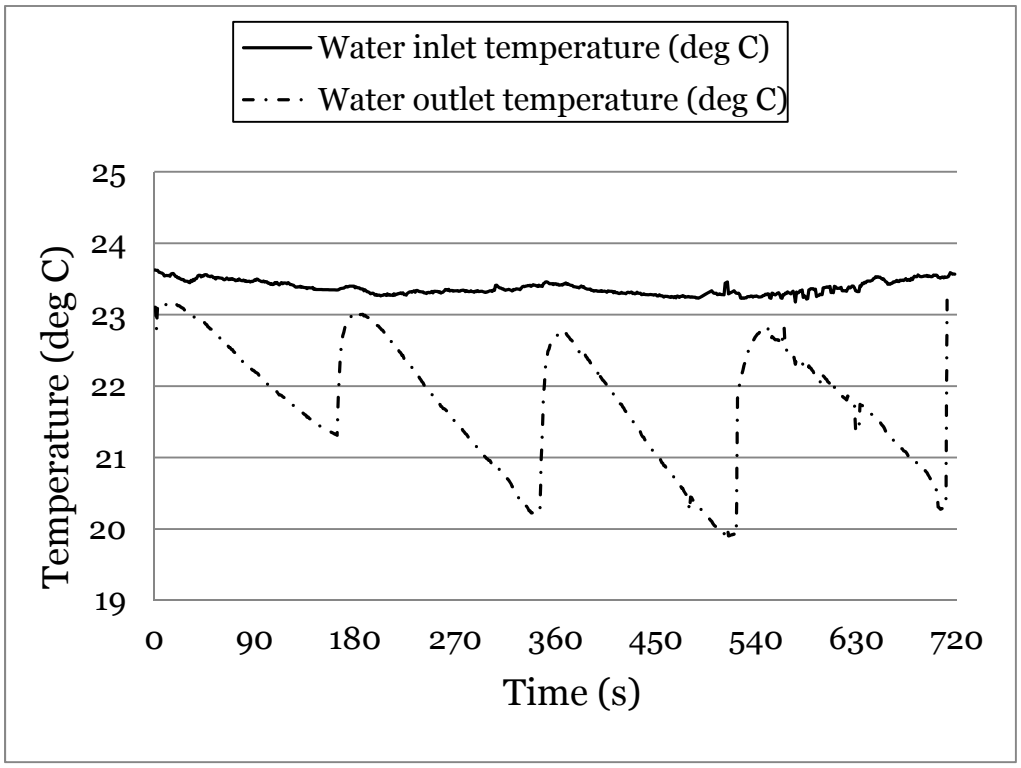

Figure 4.8. Chilled water inlet and outlet temperature variation in the heat exchanger

4.3.2. Cooling output and COP

Heat input to the system can be calculated as given in Eq. 4.1:

$$\dot{Q}_{in} = \frac{1}{t_{cycle}} \int_0^t \dot{q} dt \tag{4.1}$$

where $\dot{Q}_{in}$ is the average heat input rate, $\dot{q}$ is the instantaneous rate of heat input , and t_{cycle} is the cycle time. Heat input to the system is controlled by connecting the heating element to a VARIAC. Cooling output can be calculated by using the following expression:

$$\dot{Q}_{ref} = \frac{1}{t_{cycle}} \int_o^t \dot{m}_w C_{pw} \left(T_{in} - T_{out} \right) dt \tag{4.2}$$

where $\dot{Q}_{ref}$ is the average cooling capacity, $\dot{m}_w$ is the mass flow rate of water, C_{pw} the specific heat, and T_{in} & T_{out} are the temperatures of the water inlet and outlet respectively. Finally, the *COP* can be calculated as:

$$COP = \frac{\dot{Q}_{ref}}{\dot{Q}_{in}} \tag{4.3}$$

Using the above relations, cooling capacity and *COP* of the system is found to be 89.6 W and 0.12 respectively.

Chapter 5: Thermo-economic performance comparison of residential solar air conditioning systems

5.1. Introduction

As per the 2001 Residential Energy Consumption Survey by the US Energy Information Administration, Heating, Ventilation and Air Conditioning (HVAC) contributed about 30% of residential energy consumption in the United States [72]. This number increases to close to 35-40% for hot arid climates such as Phoenix due to its extreme summer temperatures. The conventional vapor compression systems (VCS) are prevalent in current households due to their lower initial cost, easy availability, mature technology, and high efficiency compared to their solar counterparts. However, rising electricity prices, desire for a sustainable life-style, and various government incentives are causing an unprecedented interest in alternative air conditioning systems, particularly solar-powered. The choice can be either heat-activated systems which rely on solar thermal energy, such as absorption or adsorption system, or photovoltaic-powered conventional VCS. However, the question remains as to which system is better based on the thermal performance and overall economics. The overall performance of a solar air conditioning system dependents on numerous factors such as building heating and cooling load profile, solar radiation intensity, type and size of solar collector, storage system, control scheme, etc. Due to interdependence among these factors, it is important to clearly identify the

goals of any study beforehand. The main objective of this work was to compare the thermo-economic performance of three types of solar air-conditioning systems (solar photovoltaic vapor compression, single-effect LiBr-H2O solar absorption, and silica-gel/water solar adsorption) to meet the cooling and heating demand of a 2,500 ft^2 (232 m^2) single storey, single-family residence in Phoenix, AZ, USA. Solar fraction is commonly used to evaluate the thermal performance of solar powered systems which was also used as the main criterion in the current study. The economic comparison was conducted based on the annualized system cost. Parametric studies were conducted to understand the effects of solar collector area and storage capacity on solar fraction and annualized system cost. Finally, optimum combinations of solar collector area and storage size were determined for all three systems.

The first attempt to compare solar absorption with solar vapor compression systems was published in 1981 [73]. The total energy needs of the cooling systems rather than the refrigeration cycles were taken into account. Both systems were provided with the utility grid power equal to the parasitic power requirement of solar absorption system and the rest was supplied from solar sources. It was found that *solar COP* (defined as the ratio of the total refrigeration effect and the solar radiation input) of a solar vapor compression system was in the range of 0.40 and that of the solar absorption system was around 0.25. It was also found that the initial cost of a solar cooling system is a function of both its design capacity and

the total daily cooling load to be delivered. The analysis was very limited because it did not take into account seasonal variations in the solar radiation and in the building cooling and heating load. The same author published a follow-up paper in 1983 [74] in which comparison was made based on the life-cycle cost accounting for both initial and running cost. It was found that a PV-assisted vapor-compression system could be cost-competitive with an absorption system driven by solar thermal energy. The next work on this subject was published after two decades in 2002 [75] comparing the economics of a solar-powered LiBr-H_2O vapor absorption air conditioning system (both single- and double effect) and a vapor compression system for a five-floor student hospital in Alexandra, Egypt. The typical meteorological year 2 (TMY2) weather data was used to estimate the cooling load for the building. The results showed that the double-effect vapor absorption system is the preferred option for its minimum present worth value as well as the equivalent annual cost. On the other hand, Klein and Reindl [76] concluded that only PV-driven cooling would be viable for providing sub-zero (freezing) solar refrigeration, compared with an NH_3/H_2O absorption system, and a second thermal system in which solar heat powers a Rankine cycle that in turn provides mechanical input to a vapor-compression cycle. In a somewhat similar manner, Casals [77] compared local (decentralized) solar absorption cooling with cooling provided by centralized solar thermal power plants, which generate electricity that is distributed to

conventional vapor compression units at the point of use. No clear conclusions were reached after a fairly rigorous evaluation of cost and other variables. Kim and Infante Ferreira [26] reported a comprehensive study of several solar thermal and solar PV cooling systems, based on both technical and economic considerations. Their conclusion was that solar thermal cooling, in particular a single-effect H_2O/aqueous LiBr absorption system, followed next by H_2O/silica gel adsorption and double-effect H_2O/aqueous LiBr absorption systems, are more competitive than the other solar cooling technologies, including PV-driven systems. Wang and team at SJTU published an article in 2009 [78] describing various small-scale solar powered sorption cooling systems for potential residential applications. No technical or economic analysis was performed, instead various characteristics such as performance, maintenance, and economic viability for each system types was presented. Finally, an extensive evaluation of solar cooling technologies coupled with building cooling demand for Hong Kong [79] reported that solar PV-driven systems had the greatest potential to deliver the highest annual energy savings, compared with a number of solar thermal technologies. Cost, however, did not seem to be considered in this analysis.

In summary, relatively few studies have undertaken a technical and, perhaps more importantly, an economic comparison between solar thermal and solar PV cooling systems. None of the studies relates to a residential household. Additionally, the effects of two of the most

important parameters--the size of the solar collectors and the storage capacity-were not included in any of the studies. Here, we attempt to provide answers to the following questions:

- What percentage of residential cooling and heating load can be met by various solar-powered heat pump systems for any given collector size and storage capacity?
- What is the most economical combination of the collector size and storage capacity for each type of solar heat pump system?
- Which of the solar-powered system is most economical for any given collector size and storage capacity?

In this chapter, first the methodology to calculate residential heating and cooling load is presented, followed by the simulation models for all three types of solar-powered heat pump systems. Next, a framework of the comparative study of different scenarios, including solar collector area and the storage capacity is presented. Finally, results are presented showing the thermal and economical comparison of various systems.

5.2. Cooling and heating load calculations

The single family house selected for the case study measures 2,500 ft^2 (232 m^2) in livable area and is located in Phoenix, AZ (zip code 85034). Hourly cooling and heating load profile (for 8760 hours) was calculated using eQUEST, a DOE-2 based building energy simulation tool [80]. eQUEST uses a description of the building layout, constructions, operating schedules, conditioning systems (lighting, HVAC, etc.) along with TMY2

weather data, to perform an hourly simulation of the building energy consumption. The prototype building used in the current analysis has standard construction for envelope and glazing. The entire living area was assumed to be conditioned between 4 pm to 9 am on weekdays and at all times of the day during weekends and federal holidays (typical residential occupancy). The thermostat settings during the occupied periods were fixed at 76.0 ^{o}F (24.4 ^{o}C) and 71.0 ^{o}F (21.7 ^{o}C) and during the unoccupied period were fixed at 82.0 ^{o}F (27.8 ^{o}C) and 64.0 ^{o}F (17.8 ^{o}C) during the cooling and heating seasons, respectively [81]. The effect of installing roof-top solar collectors on heat transfer across the roof is not taken into account because it is expected to affect all systems equally. Figure 5.1 shows the house prototype created in eQUEST. Figure 5.2 depicts the monthly heating and cooling load profile generated by eQUEST. It is clear that July and August requires the most cooling and December and January the most heating. The cooling and heating load in Figure 5.2 does not include parasitic loads, such as those to run ventilation fans. Figure 5.3 shows the electricity consumption, if cooling and heating was provided by a heat pump unit with a Seasonal Energy Efficiency Ratio (SEER) rating of 10.0 and the Heating Seasonal Performance Factor (HSPF) of 7.7.

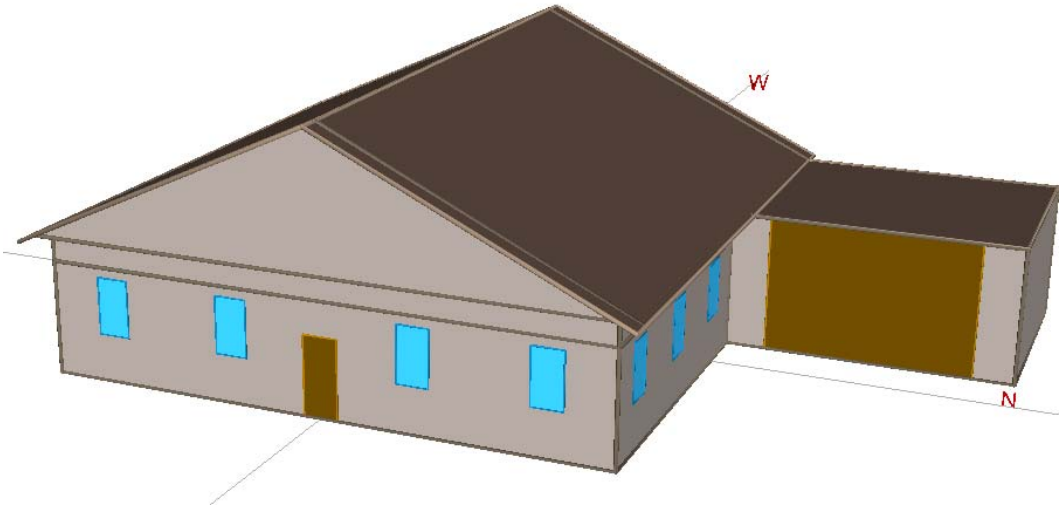

Figure 5.1. Single family house prototype in eQUEST

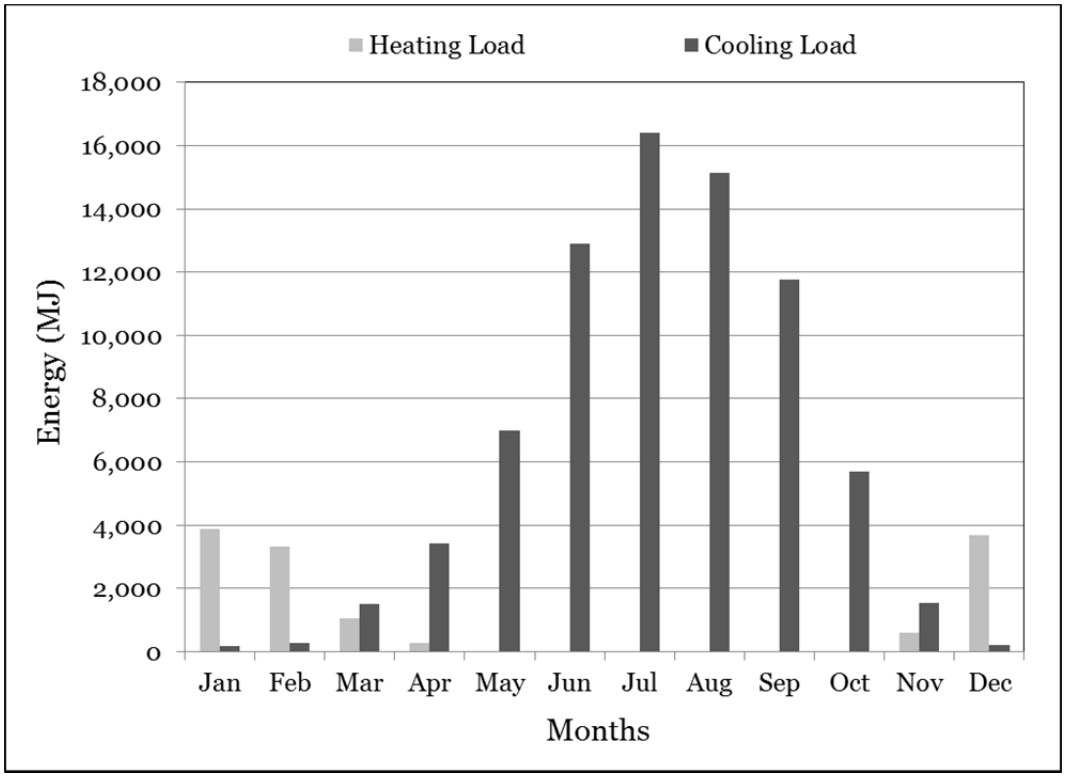

Figure 5.2. Monthly heating (heat addition) and cooling (heat removal) load profile

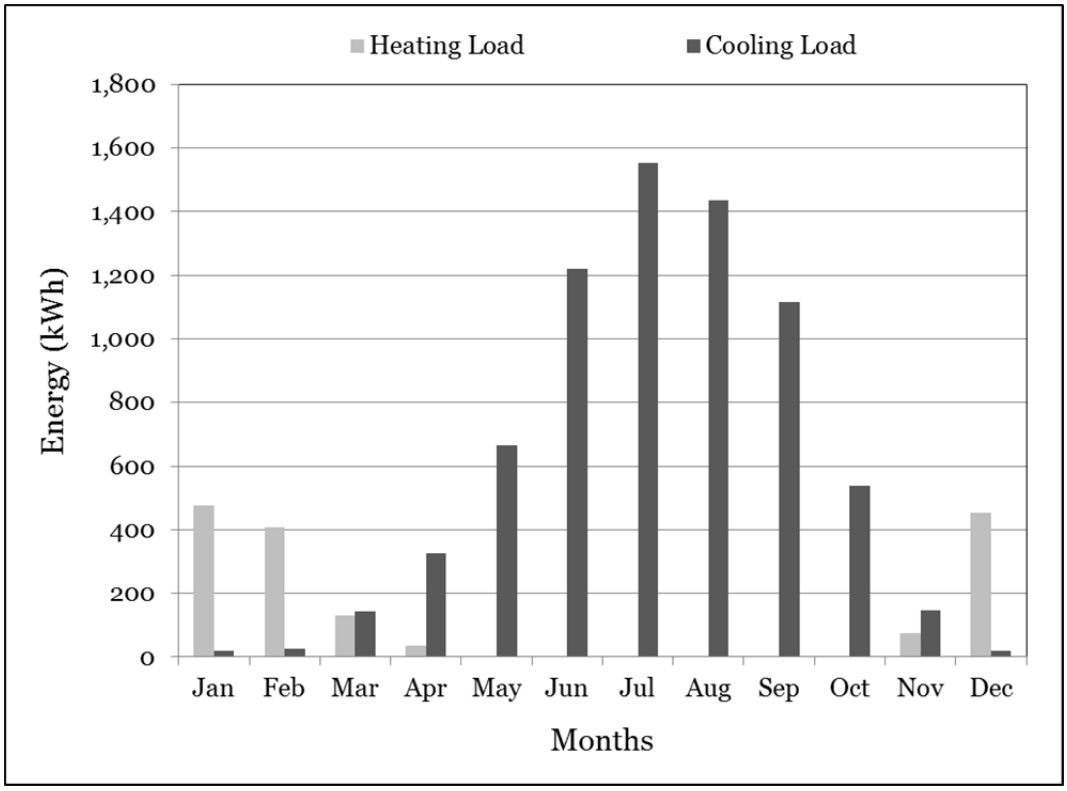

Figure 5.3. Monthly heating and cooling energy consumption profile, assuming an electric heat pump with SEER = 10.0 and HSPF=7.7

5.3. Description of solar thermal systems

5.3.1. System configuration

The complete system layout for both adsorption and absorption systems (also referred together as "sorption system" in this chapter) is illustrated in Figure 5.4. It includes a solar system collector array, a thermal storage tank, an adsorption/absorption heat pump unit, and an auxiliary heat supplying unit such as a gas heater. There are three different loops in the system: the solar collection loop between the solar collector and the thermal storage tank, the hot water loop between the storage tank

and the heat pump, and the chilled air loop between the heat pump and the conditioned space. The auxiliary heating is provided by a gas heater.

Options for the solar collector can vary significantly in complexity. These options can be roughly categorized as the following: flat plate, evacuated tube, and concentrating collectors. In order to choose between these, one must define the temperatures needed to run the solar thermal heat pump system. Silica-gel water adsorption systems can operate at a driving temperature as low as 55 ^{o}C and at a COP of 0.5 [27]. Technically, all three types of collectors can provide this driving temperature, but flat-plate collectors were chosen for the adsorption system because they are relatively cheaper. Single-effect LiBr-H_2O absorption systems can operate at a driving temperature as low as 75 ^{o}C at a COP of 0.75 [27]. The flat-plate collectors will not be able to provide this temperature for a significant part of the year. Hence, evacuated tube collectors were chosen for absorption system.

The thermal storage tank used in the analysis is a standard cylindrical tank with a length-to-diameter ratio of 2.0. The maximum temperature of the hot water in the storage tank was limited to 95 ^{o}C to avoid any potential safety issues due to above atmospheric pressures as this system is installed in a residential setting.

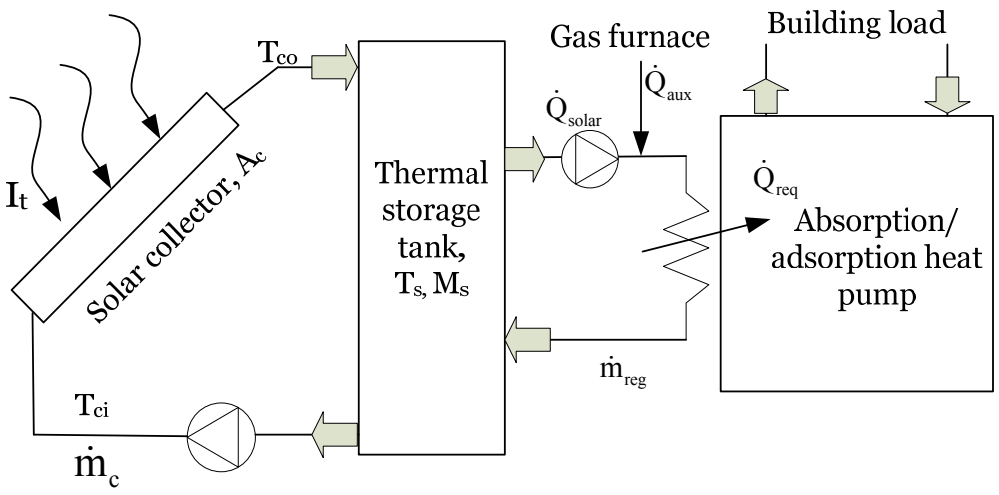

Figure 5.4. Schematic of solar thermal adsorption/absorption heat pump

5.3.2. Mathematical modeling and simulation

The TMY2 hourly mean incident solar radiation data for Phoenix were obtained from the National Solar Radiation Database [82]. The average hourly efficiency of both flat-plate and evacuated-tube collectors was calculated using Eq. 5.1 [83]:

$$\left[\eta_{tc}\right]_i = \left[a_o - a_1 \frac{T_m - T_a}{I_t} - a_2 \frac{\left(T_m - T_a\right)^2}{I_t} \right]_i \tag{5.1}$$

where i is the number of hours (1,2,.....8760), η_{tc} the thermal collector efficiency, T_m the mean collector temperature, I_t the total solar radiation, and T_a the ambient temperature. The constants a_o, a_1, and a_2 are obtained experimentally and depends on collector geometry and type. For our analysis we chose the following constants to represent selected commercial evacuated tube (Apricus 30) and flat plate (AE-40) collectors, respectively:

a_o = 0.39 and 0.69, a_1 = 0.83 and 3.39, a_2 = 4.7 x 10^{-3} and 1.9 x 10^{-3} [84, 85]. The reference provides constants based on the absorber area which was then converted to gross area.

Mean collector temperature was calculated by averaging the collector inlet and exit temperatures as shown in Eq. 5.2:

$$\left[T_m\right]_i = \left[\frac{T_{in} + T_{out}}{2}\right]_i \tag{5.2}$$

where T_{in} is the collector inlet temperature and T_{out} the collector exit temperature. The useful heat and exit temperature from the collector were calculated using Eqs. 5.3 and 5.4 respectively.

$$\left[\dot{Q}_u\right]_i = \left[F\eta_{tc} I_t\right]_i A_{tc} \quad \text{where} \begin{cases} \text{F=0 if } \eta_{tc} \le 0 \\ \text{F=1 if } \eta_{tc} > 0 \end{cases} \tag{5.3}$$

$$\left[T_{out}\right]_i = \left[T_{in} + \frac{\dot{Q}_u}{\dot{m}_{tc} A_{tc} C_{pw}}\right]_i \tag{5.4}$$

where $\dot{Q}_u$ is the useful heat, A_{tc} the area of the thermal collector, $\dot{m}_{tc}$ the mass flow rate of water through collector, and C_{pw} the specific heat of water. F is a flag which turns-off the circulation pump in the collector loop when collector efficiency drops below zero to avoid cooling of the storage water.

The water temperature in the thermal storage tank at any hour can be evaluated from Eq. 5.5:

$$M_s C_{pw}\left(\frac{dT_s}{di}\right) = \left[\dot{Q}_u - \dot{Q}_{solar} - U_s A_s (T_s - T_a)\right]_i \tag{5.5}$$

where M_s is the mass of water in the storage tank which is calculated by dividing the storage volume by the water density, T_s the temperature of water in the storage tank, U_s the overall coefficient of heat loss from the storage tank, and A_s the surface area of the storage tank. $\dot{Q}_{solar}$ is the solar heat contribution to operate the sorption machine. By applying the finite difference method and considering an unstratified tank, the water temperature in the storage tank can be calculated as shown in Eq. 5.6:

$$T_s^{i+1} = T_s^{i} + \frac{\left[\dot{Q}_u - \dot{Q}_{solar} - (UA)_s(T_s - T_a)\right]_i}{M_s C_{pw}} \tag{5.6}$$

where T_s^{i+1} is the temperature of the water in the storage tank at hour equal to $i + 1$ and T_s^{i} the temperature of the water at hour i.

The total heat required to run the thermal air conditioning machine is equivalent to the total cooling and heating load divided by the coefficient of performance (COP) of the machine. Additionally, the total required heat is provided first from the storage tank (solar component) and if necessary, the remainder from the gas heater as formulated in Eq. 5.7:

$$\left[\dot{Q}_{req}\right]_i = \left[\frac{\dot{Q}_{cool} + \dot{Q}_{heat}}{COP}\right]_i = \left[\dot{Q}_{solar} + \dot{Q}_{aux}\right]_i \tag{5.7}$$

where $\dot{Q}_{req}$ *is* the required heat, $\dot{Q}_{cool}$ the heat to be removed from the conditioned space, $\dot{Q}_{heat}$ the heat to be delivered to the conditioned space, and $\dot{Q}_{aux}$ the auxiliary heat provided by the gas heater to meet the heating

requirement. For the simplicity of the analysis, the cooling and heating COP of the sorption systems is assumed the same because that's how it is typically reported in the literature [25, 27].

The maximum useful heat in the storage tank which can be supplied to the sorption system is a function of the regenerator heat exchanger effectiveness, storage temperature, and the minimum driving temperatures of the sorption system:

$$\left[\dot{Q}_{av}\right]_i = \left\{ \begin{array}{ll} \varepsilon \dot{m}_{reg} C_{pw} (T_s - T_{\min}) & if\ \mathrm{T_s} > \mathrm{T_{min}} \\ 0 & if\ \mathrm{T_s} \le \mathrm{T_{min}} \end{array} \right\}_i \tag{5.8}$$

where $\dot{Q}_{av}$ *is* the maximum useful heat in the storage tank, ε the regenerator heat exchanger effectiveness, $\dot{m}_{reg}$ the mass flow rate through the regenerator, and T_{min} the minimum driving temperature of the sorption system.

The solar heat contribution is calculated as:

$$\left[\dot{Q}_{solar}\right]_i = \left\{ \begin{array}{ll} \dot{Q}_{av} & if\ \ \dot{Q}_{av} \le \dot{Q}_{req} \\ \dot{Q}_{req} & if\ \ \dot{Q}_{av} > \dot{Q}_{req} \end{array} \right\}_i \tag{5.9}$$

Finally, two temperature conditions were applied as shown in Eqs. 5.10 and 5.11. First, the maximum temperature in the storage tank cannot exceed 95 ^{o}C and second, the inlet temperature to the solar collector is equal to the water temperature in the storage tank:

$$\left[T_s\right]_{i\max} = 95\ ^{o}\mathrm{C} \tag{5.10}$$

$$[T_{in}]_i = [T_s]_i \tag{5.11}$$

The above sets of equations (5.1 to 5.11) were solved explicitly in Matlab for i=1 to 8760 hours. A flow chart of the simulation program is given in Figure 5.5. Table 5.1 shows the values of different parameters used in the sorption system simulation.

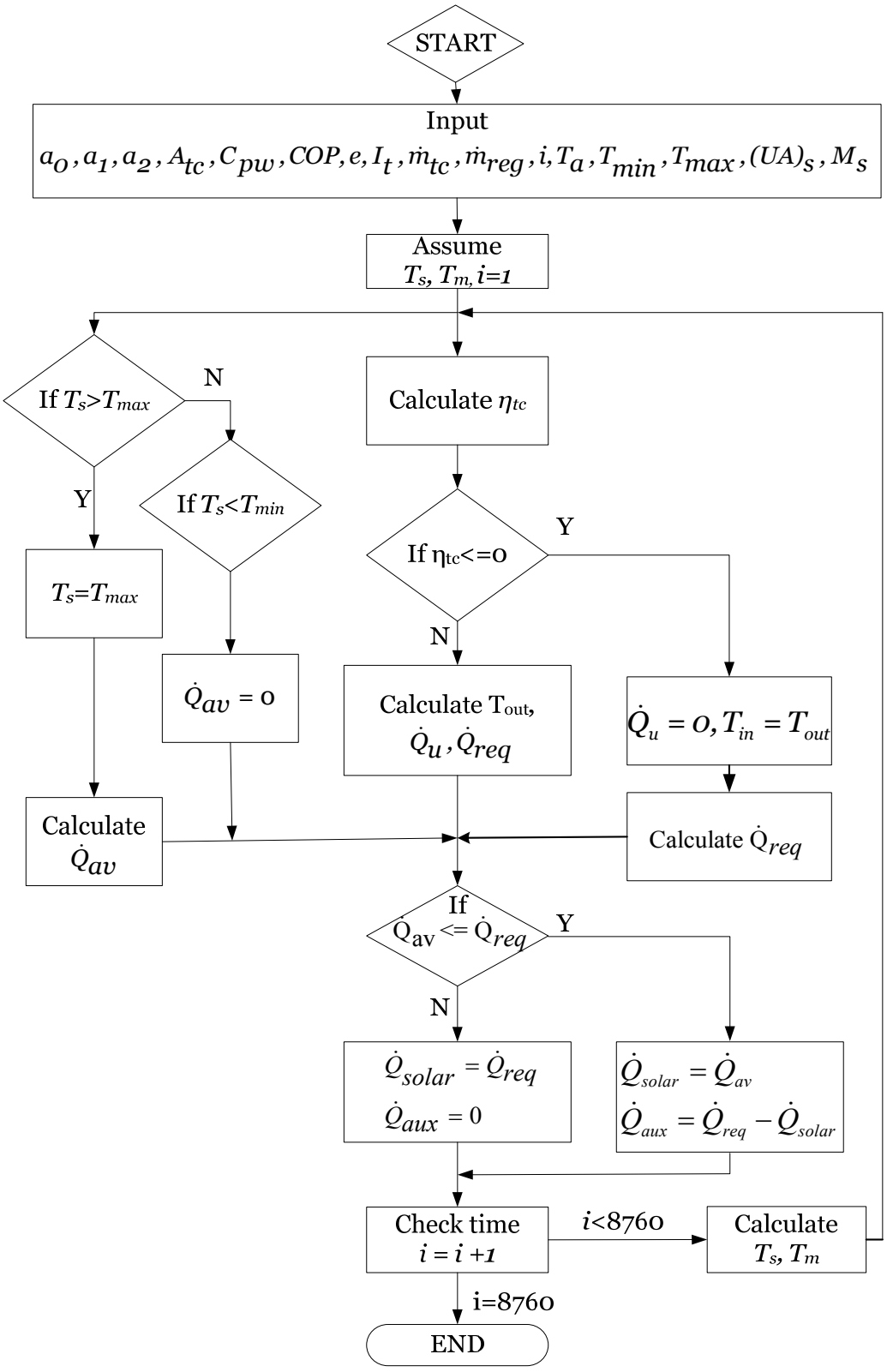

Figure 5.5. Solar thermal systems simulation program flow chart

Table 5.1. List of parameters and their values used in the sorption system simulation

Parameters	Value (adsorption/ absorption)	Unit
Zero-loss efficiency, a_o	0.69/0.39	
1st order heat loss coefficient, a_1	3.39/0.83	
2nd order heat loss coefficient, a_2	0.0019/0.0047	
Coefficient of performance, *COP*	0.50/0.75	
Density of water, ρ	1,000	kg m^{-3}
Mass flow rate in the storage-regenerator loop, $\dot{m}_{reg}$	0.40	kg s^{-1}
Maximum thermal storage tank temperature, T_{max}	95	^oC
Minimum driving temperature, T_{min}	55/75	^oC
Reference ambient temperature, T_o	25	^oC
Regenerator heat exchanger effectiveness, ε	0.7	
Specific mass flow rate in the collector-storage loop, $\dot{m}_c$	0.02 [79]	kg s^{-1} m^{-2}
Specific heat of water, C_{pw}	4.186	kJ kg^{-1} $^oC^{-1}$
Thermal storage tank overall heat loss coefficient, U_s	0.2837 [83]	kW m^{-2} $^oC^{-1}$

5.4. Description of solar photovoltaic system

5.4.1. System configuration

As shown in Figure 5.6, the solar electric system is comprised of four major components: PV modules, inverter, battery, and vapor

compression heat pump unit. The system is similar to the conventional residential units except the source of electricity, which is solar PV array in this case. The battery storage in the solar PV system plays a similar role as the thermal storage tank in sorption systems. The heat pump used in the study is the YHJD LX series model manufactured by York [86]. The SEER for the heat pump is 13. The heating seasonal performance factor (HSPF) of the heat pump is 9.0. The HSPF is the ratio of the total thermal output (in British Thermal Units) to the electricity (in Watt-hour) consumed during a normal heating season.

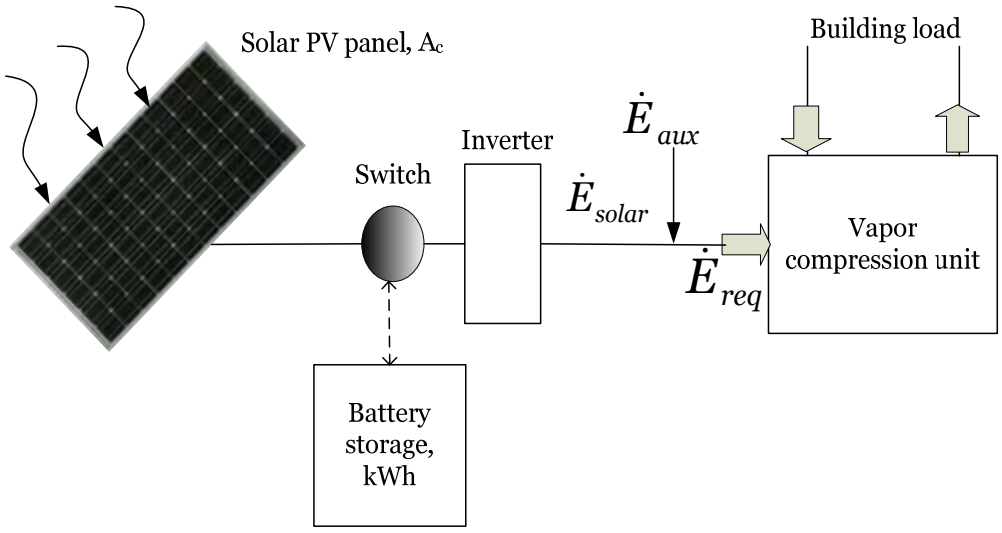

Figure 5.6. Configuration of solar PV heat pump

5.4.2. Mathematical modeling and simulation

The hourly mean kWh energy outputs from photovoltaic panels were obtained from the PVWatts calculator developed by the National Renewable Energy Laboratory (NREL) [87]. Using the TMY2 weather data for the selected location, the PVWatts calculator determines the solar

incident radiation of the PV array and the PV cell temperature for each hour of the year. The Direct Current (DC) energy for each hour is calculated from the PV system DC rating and the incident solar radiation and then corrected for the PV cell temperature. The AC energy for each hour is calculated by multiplying the DC energy by the overall DC-to-AC derate factor and adjusting for inverter efficiency as a function of load. PVWatts uses a default derate factor of 0.77 which is also used in this analysis. The maximum Depth of Discharge (DOD) of the battery bank is assumed to be 0.8 [88]. The DOD refers to the amount of energy that has been removed from a battery (or battery pack) and usually expressed as a percentage of the total capacity of the battery. The solar PV simulation is set-up in a way that primary source of the electricity to run the heat pump is obtained from the solar system and any auxiliary demand is met by the grid power. Table 5.2 shows the values of different parameters used in the solar PV system simulation.

Table 5.2. List of parameters and their values used in the solar PV heat pump simulation

Parameter	Value	Unit
DC to AC derate factor, df	0.77	-
Battery maximum depth of discharge, DOD	0.8	-
Heat pump SEER rating	13.0	-
Heat pump HSPF rating	9.0	-

5.5. Thermal performance comparison criteria

The sizing of a solar heat pump system depends on many subsystems including the heat pump unit, solar collector array, storage system, etc. Typically, a heat pump unit is sized to meet the peak building load, however sizing the solar collector array and storage system to meet the residential peak load is either not possible or prohibitively expensive. The reason is that meeting peak building cooling load in hot climates like Phoenix using 100% solar energy requires collector and storage sizes exceeding the available roof/floor area. But due to different operating characteristics, it is natural to ask which of the three systems can provide higher solar contribution for a given collector and storage size. Solar contribution was measured as *solar fraction (SF)*. The *SF* is the portion of solar energy contribution as compared to the total energy required to drive the heat pump unit. In this study, the *SF* is defined below in Eqs. 5.12 and 5.13:

For solar PV heat pump system,

$$SF = \frac{\sum_{i=1}^{m} \dot{W}_{solar}}{\sum_{i=1}^{m} \dot{W}_{req}} \tag{5.12}$$

For solar thermal heat pump system,

$$SF = \frac{\sum_{i=1}^{m} \dot{Q}_{solar}}{\sum_{i=1}^{m} \dot{Q}_{req}} \tag{5.13}$$

where $\dot{W}_{solar}$ is the solar electric gain from PV panels, $\dot{W}_{req}$ the total energy required to drive the heat pump, and *m* the total number of time steps.

5.6. Economic analysis

5.6.1. Costs components

The total cost of any system consists of three main components, namely the initial cost, the operating cost, and the maintenance cost. The following section describes each of these components as relates to the current study.

5.6.1.1. Initial cost

The main components of a solar thermal heat pump considered in the initial costs calculation include the solar collector array, the thermal storage tank, the auxiliary gas heater, and the sorption heat pump unit. Additional equipment such as circulation pumps, piping, controls, are not considered because they are relatively less expansive and the difference in their costs between the three systems can be assumed to be negligible.

The initial cost of a flat plate and an evacuated tube solar collector was estimated to be about \$209/m^2 and \$279/m^2 of gross collector area respectively [89]. The cost of thermal storage tanks is primarily a function of the tank size - however, it can also depend on the manufacturer, type, and quality of the storage tank material. Also, costs for all tank sizes included in this study were not available on any of the vendor's website. Based on the available prices on the web for different sizes of tanks [90] and quotes received from one of the manufacturer [91], a linear curve was

fitted to estimate prices of any intermediate tank size. Eq. 5.14 shows the storage tank cost function used in the analysis:

$$CI_s = 779.11 \times V_s + 264.96$$

$$\text{for } 75 \text{ gallons } (0.284\ m^3) < V_s < 11{,}60 \text{ gallons } (4.391\ m^3) \quad (5.14)$$

where CI_s is the initial cost of thermal storage tank and V_s the storage tank volume.

The gas heater was sized in a way that it can provide the maximum heat rate required during a year to meet the auxiliary thermal energy requirement. The initial cost of the gas heater was assumed to be $1,000 per therm capacity [92]. Sorption heat pump cost is difficult to estimate, since with the exception of some absorption systems, not many residential-scale systems are in the market. Therefore, conservatively the initial cost for an adsorption/absorption unit was assumed to be $20,000.

The main components of a solar PV system include the PV module, battery bank, inverter, and a vapor compression heat pump unit. The associated costs for each component were obtained from a variety of references that compile average prices.

For the PV module, not including the inverter, initial costs was estimated at $4,800/kW [93]. Inverter cost was obtained from multiple sources and found to be about $1,000/kW [94, 95]. Electrical energy storage cost for battery storage was estimated at $150/kWh [96]. The cost of a 5 ton air source heat pump unit was estimated at $5,350 [97].

Table 5.3 shows the estimated initial costs for all three systems. It also lists useful life span of all the components.

5.6.1.2. Operating cost

Operating costs include the cost of natural gas for solar thermal systems and cost of grid electricity for the solar PV system. The small amount of electricity required to operate pumps in the thermal collector loop, regenerator loop, and for the absorption machine was neglected in the analysis. The annual operating cost of thermal systems was calculated by multiplying the unit gas cost and the annual gas consumption:

$$CO_{ts} = GC\, x \frac{\sum_{i=1}^{8760} \dot{Q}_{aux}}{EF} \tag{5.15}$$

where CO_{th} is the operating cost of the thermal systems, GC the unit gas costs, and EF the energy factor. Energy factor is an overall efficiency rating of the gas water heater and is assumed to be 0.9 in this analysis. The natural gas cost was assumed to be $1.17/therm in this analysis [98]. To estimate the operating cost of the solar PV system, the average cost of electricity was assumed to be $0.12/kWh [99].

5.6.1.3. Maintenance cost

The maintenance cost depends on a large number of variables such as local labor rates, labor experience, equipment run time, etc. Considering that these are small-scale residential systems, maintenance cost can be assumed to be negligible compared to the initial and operating cost.

Additionally, the difference between the three systems can be assumed to be minimal. Hence, the maintenance cost was neglected in this analysis.

Table 5.3. Component costs used in the economic analysis of the three systems

Component	Cost	Unit	Useful Life
Solar adsorption system			
Thermal heat pump	$20,000	$/unit	15
Collector (flat plate)	$209	$/m^2	20
Storage tank	Eq. 5.12	$/m^3	20
Gas heater	$1,000	$/therm	20
Natural gas	$1.17	$/therm	-
Solar absorption system			
Thermal heat pump	$20,000	$/unit	15
Collector (evacuated)	$279	$/m^2	20
Storage tank	Eq. 5.12	$/m^3	20
Gas heater	$1000	$/therm	20
Natural gas	$1.17	$/therm	-
Solar photovoltaic system			
Air source electric heat pump	$5,350	$/unit	15
Photovoltaic collector	$4,800	$/kW	20
Battery	$150	$/kWh	7
Inverter	$1000	$/kW	10
Electricity	$0.12	$/kWh	-

5.6.2. Economic comparison criteria

Several economic criteria have been proposed and used for evaluating solar energy systems, and there is no universal agreement on which should be used [83]. The present worth cost (PWC) [100] and equivalent annual cost (EAC) [75] methods are normally used to evaluate the life-cycle costs of HVAC systems. The EAC comparison method is one of the most convenient methods, particularly for systems that are composed of several subsystems with unequal life spans. This work utilizes the EAC method because subsystems in both sorption system and solar PV system have unequal useful life spans. With the EAC method, all the costs occurring over a period are converted to an equivalent uniform yearly amount. This method does not require the assumption of replacement of a system.

The EAC for sorption system is the summation of the EAC values for the thermal collector, storage tank, gas heater, absorption/adsorption heat pump, and the annual operating cost:

$$EAC_{ts} = EAC_{tc} + EAC_{s} + EAC_{gh} + EAC_{thp} + CO_{ts} \quad (5.16)$$

where *EAC* represents the equivalent annual cost and the subscripts ts, *tc, s, gh,* and *thp* represents thermal system, thermal collector, storage tank, gas heater, and thermal heat pump respectively.

The EAC for solar PV system is the summation of the EAC values for the solar photovoltaic, Battery storage, inverter, VCS heat pump, and the annual operating cost:

$$EAC_{spv} = EAC_{pv} + EAC_{batt} + EAC_{inv} + EAC_{hp} + CO_{spv} \quad (5.17)$$

where subscripts *spv*, *pv, batt, inv,* and *hp* represents solar PV air conditioning system, photovoltaic collector, battery storage, inverter, and conventional heat pump respectively. Equation 5.18 was used to calculate the EAC:

$$EAC = CI\left[\frac{r(1+r)^N}{(1+r)^N - 1}\right] \quad (5.18)$$

where *CI* is the initial cost, *r* the interest rate, and *N* the life span of components. The interest rate was assumed to be 8% in this analysis.

5.7. Results and discussion

5.7.1. Thermal performance comparison

As explained in section 5.1, the objective here is to compare the thermal performance based on solar fraction of solar thermal and solar PV heat pump systems as a function of collector size and the storage capacity. The collector for the thermal systems is the solar thermal collector array and for the electric system the PV array, and their size is defined as the surface area directly exposed to the solar radiation. The storage capacity is difficult to compare. The electric system in this analysis stores energy as electric charge in a battery bank, whereas thermal systems store energy as hot water in a thermal storage tank. Considering the different nature of storage, it was determined that "exergy capacity" is a better parameter to compare the storage capacity of each system. For the electric system,

electricity storage capacity is the same as the "exergy capacity". For thermal systems, the "exergy capacity" is defined as follows:

$$Ex_s = M_s C_{pw}(T_s - T_0) * \left[1 - \frac{T_0}{T_s}\right] \tag{5.19}$$

where Ex_s is the exergy capacity of the thermal storage system and T_o the reference temperature (assumed 25 ^oC = 298 K in this analysis).

Figure 5.7 shows the monthly annual profiles of solar fraction for different systems at a fixed collector area of 50 m^2 and exergy storage capacity of 25 kWh. The first important observation from Figure 5.7 is that except for a few months in a year (March, April, and November), none of the solar systems is capable of providing 100% of the required energy. Solar fraction is as low as 35-40% for the thermal systems and 45% for the electric system during the summer peak months of July and August. Also, the solar PV system provides maximum solar fraction among all systems for every month of the year. Generally, the solar fraction is less than one, indicating that just the solar electric or thermal gain acquired from the solar collectors is not sufficient to fully drive the respective solar heat pump systems.

Figure 5.8 shows a three-dimensional plot to demonstrate the effect of the storage capacity and the collector area on annual average solar fraction for the adsorption heat pump. As can be seen here, the solar fraction increases by increasing the collector area but the rate of increase decreases continuously. Figure 5.9 and Figure 5.10 show the effect of

increasing the exergy storage capacity and the collector area respectively on annual average solar fraction for all three systems. Due to the lower COP of thermal systems, their annual average solar fraction is mostly inferior to the solar electric system. The lower COP means the same exergy storage capacity provides less cooling and heating to the building. However, solar adsorption performs better compared to the absorption system because it can provide cooling at lower generation temperatures.

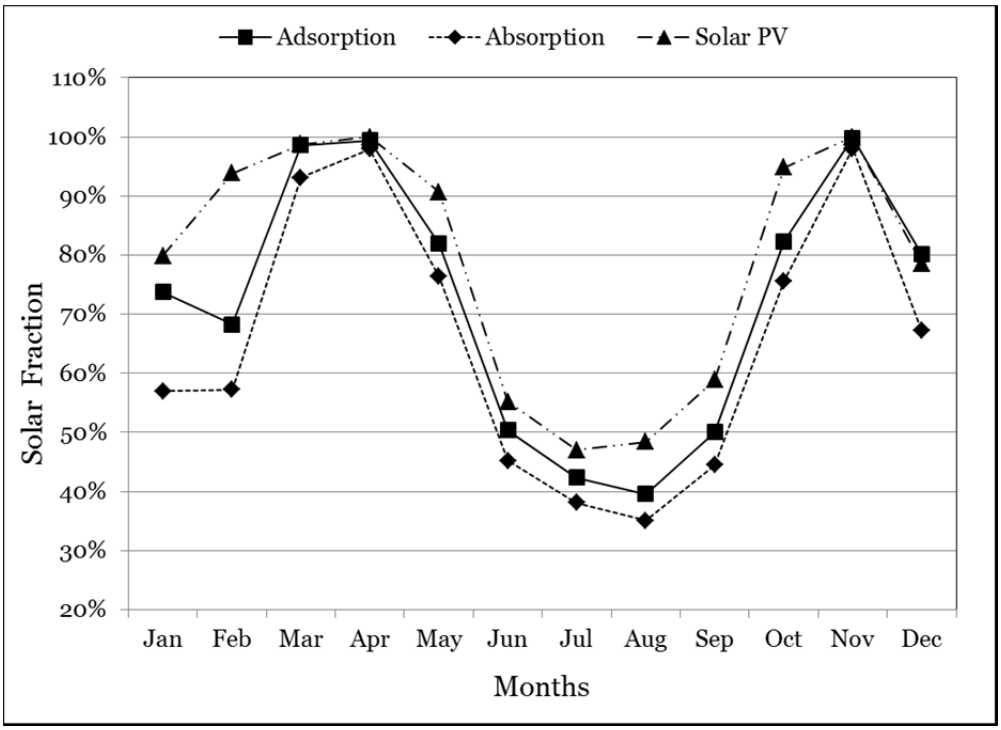

Figure 5.7. Monthly solar fraction of the combined cooling and heating energy requirement at a fixed collector area of 50 m² and exergy storage capacity of 25 kWh

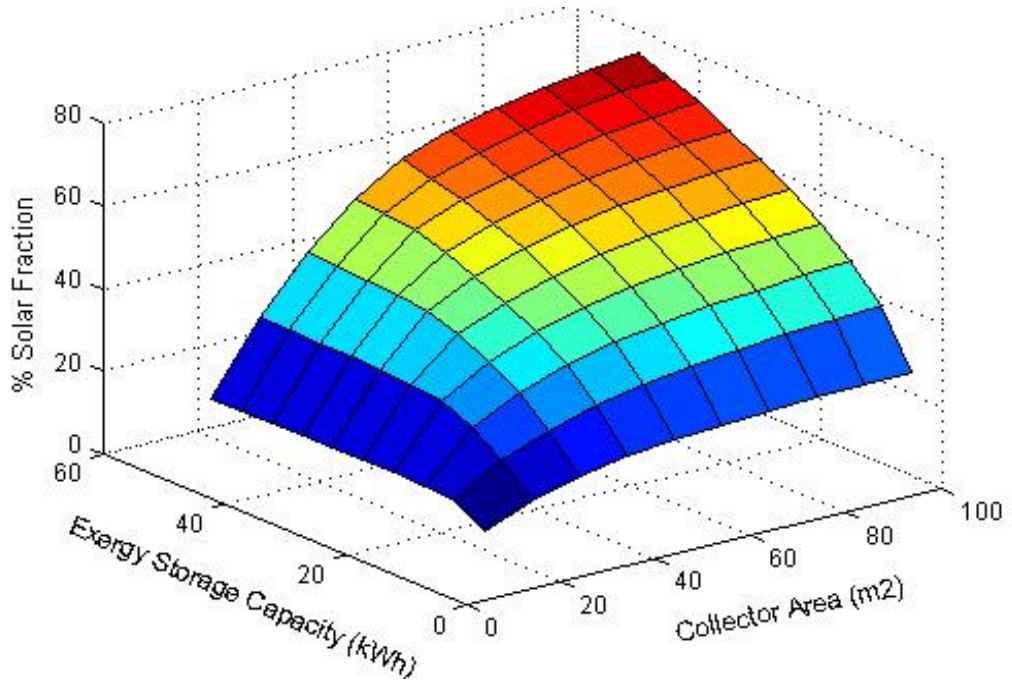

Figure 5.8. Effect of the collector area and storage capacity on annual solar fraction for an adsorption heat pump

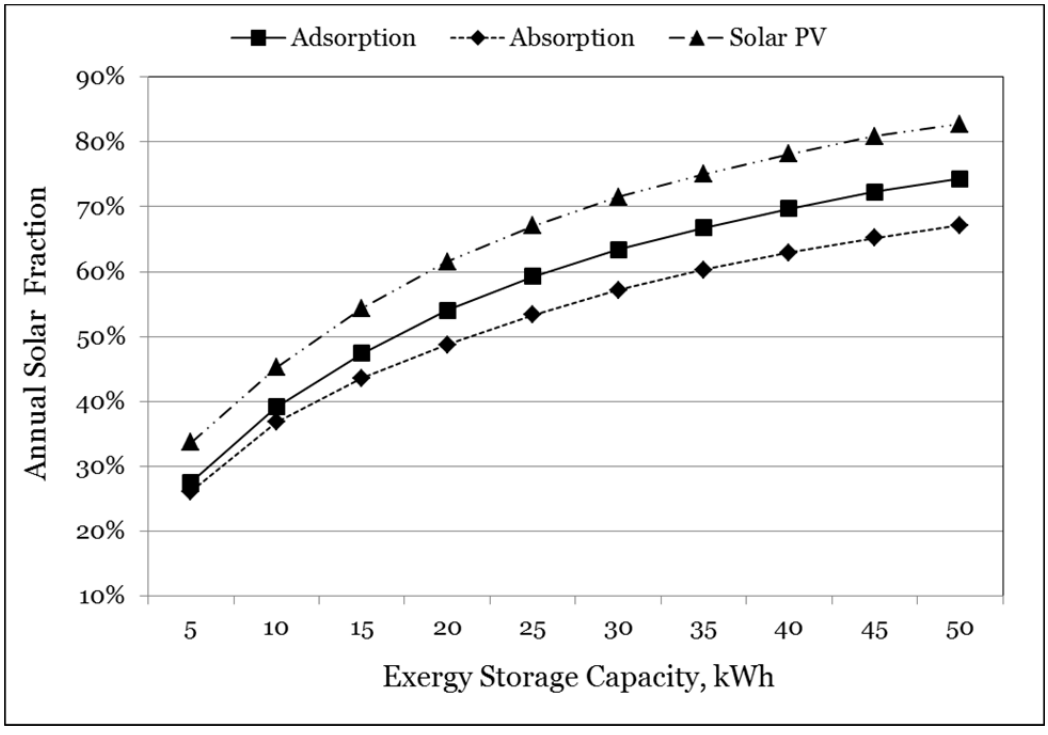

Figure 5.9. Effect of storage capacity on annual solar fraction at fixed solar collector area of 50 m²

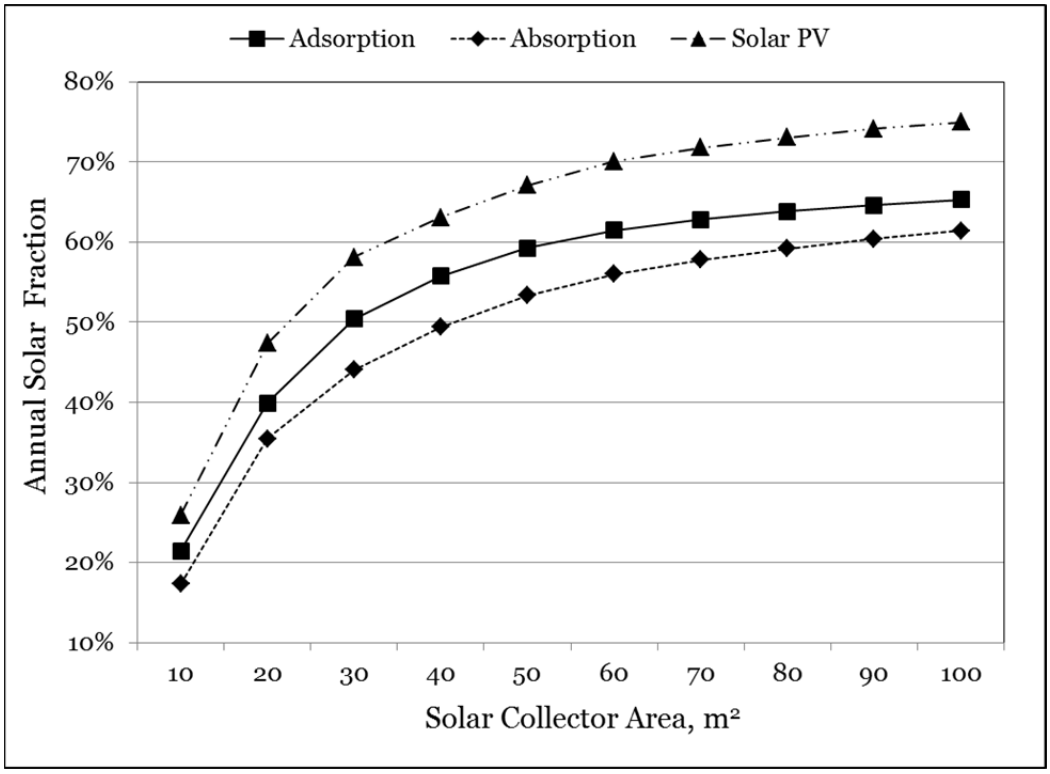

Figure 5.10. Effect of solar collector area on annual solar fraction at a fixed exergy storage capacity of 25 kWh

5.7.2. Economic comparison

Comparing the annualized cost contribution due to initial and operating costs for each component reveals some interesting results as shown in Figure 5.11. The comparison is based on a fixed collector area of 50 m² and a fixed exergy storage capacity of 25 kWh. Whereas the solar fraction of the solar PV system is almost always better, the annualized cost of running a thermal system is slightly better. This is due to the relatively higher cost of solar PV arrays compared to the solar thermal collectors. Additionally, the storage cost is also higher for the electric system. To be competitive with the solar thermal systems, PV panel prices must drop by about 30%. However, initial cost of the heat pump unit for thermal

systems is almost four times higher compared to the electric system and future success of these systems strongly depends on reducing the initial cost. As expected, the annualized cost of a conventional VCS heat pump powered by utility grid is significantly better. If solar thermal systems need to be competitive with the conventional VCS then prices for thermal collector and thermal heat pump unit (assuming all other prices remain same) must drop by about 70%. If solar PV system needs to be competitive with the conventional system then prices for photovoltaic panel, battery storage, and inverter must drop by about 75-80%. If comparison is based on the % GHG reduction, then based on the Greenhouse Gas (GHG) emission factors for the electricity in the AZNM region [101] and for natural gas [102], the adsorption system reduces GHG emissions by 19%, absorption system by 38%, and solar PV system by 67%.

Similar conclusions can be drawn from Figure 5.12 which shows the variation in annualized total cost as a function of the storage capacity at a fixed solar collector area of 50 m^2. It turns out that solar PV is more expansive than either of the thermal systems. However, which one of the solar systems is better depends on the range of storage capacity. Below 20 kWh storage capacity, absorption is a better option and above that adsorption. This can be explained by the fact that smaller storage capacity results in higher storage temperature required to drive the absorption system. Since an adsorption system requires lower driving temperature, a larger storage will be more economical.

If the solar collector area is increased and the storage capacity is kept fixed at 25 kWh, the results in Figure 5.13 show that each system has their best performance in a certain operating range. The solar electric system fares better below 30 m², absorption system between 30 – 40m², and the adsorption system above that. This trend is due to the relative cost of the solar collectors for all three systems. Due to fixed storage capacity, the additional solar collector area may increase the cost linearly but does not increase the cooling output in the same ratio. The Solar PV array being most expensive makes the solar PV system higher cost at larger collector area.

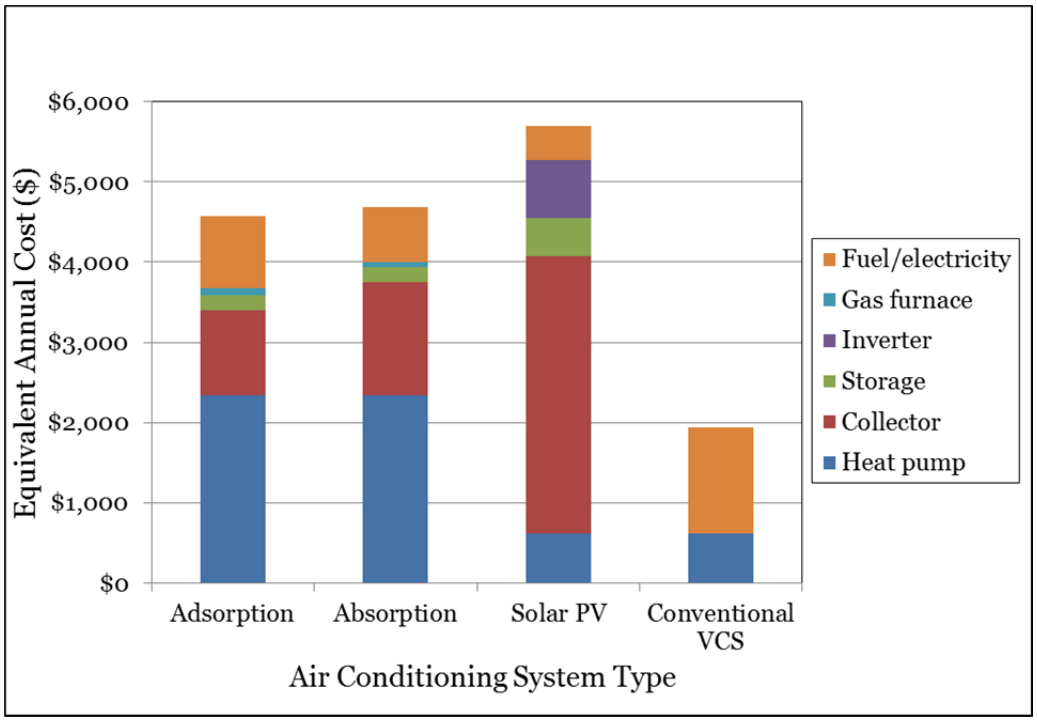

Figure 5.11. Annualized component costs for three systems at a fixed collector area of 50 m² and exergy storage capacity of 25 kWh

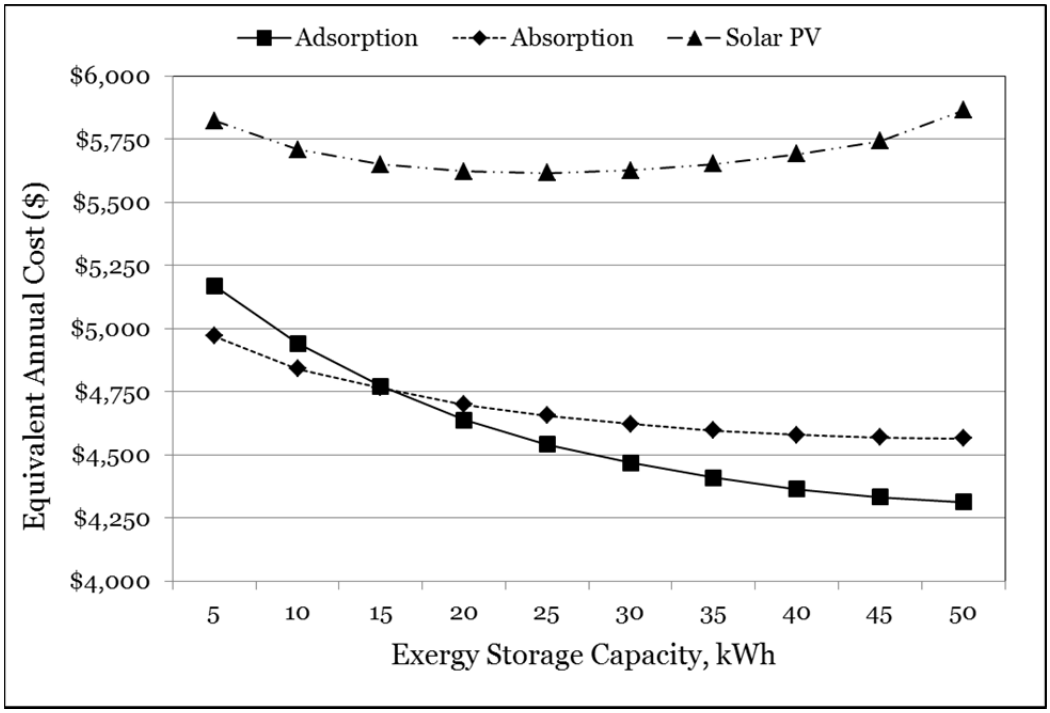

Figure 5.12. Effect of storage capacity on annualized system cost at a fixed collector area of 50 m²

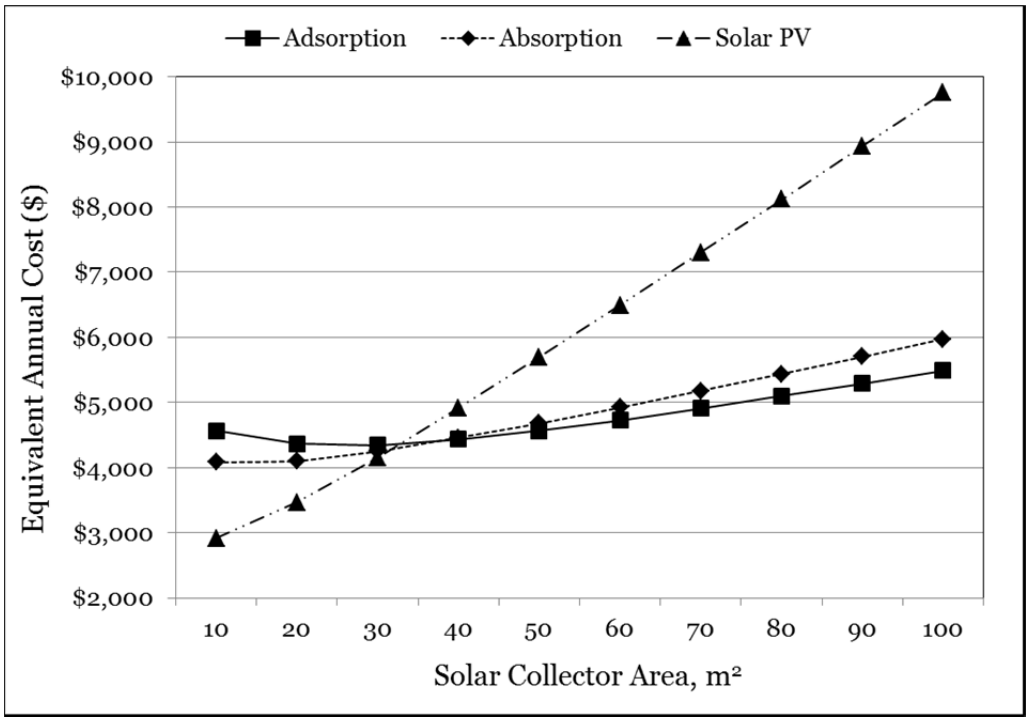

Figure 5.13. Effect of the solar collector area on annualized system cost at a fixed exergy storage capacity of 25 kWh

Table 5.4 shows the optimum combination of collector area and exergy storage capacity and corresponding EAC for all three types of systems. The solar PV system has the lowest EAC and adsorption the highest. However, adsorption system also has the highest solar fraction and hence smallest need for the auxiliary energy. The last column also shows the %GHG reduction compared to the conventional VCS. The negative %GHG reduction for the absorption unit is due to higher emissions from natural gas burning in the auxiliary gas heater compared to emissions associated with electricity for the AZNM region. Due to only 17% solar fraction for the absorption unit, remaining 83% energy is provided by the natural gas powered heating.

Table 5.5 shows that if the minimum solar fraction is limited to 50% then the EAC for all three systems is almost equal except the fact that adsorption system provides about 20% more solar contribution.

Table 5.4. Optimum combination of collector area and storage capacity

System type	Collector area (m^2)	Storage capacity (kWh)	Equivalent annual cost ($)	Solar fraction	% GHG reduction
Adsorption	40	40 (≈682 gallons)	$4,268	65.0%	30.4%
Absorption	10	10 (≈170 gallons)	$3,992	17.1%	-9.7%
Solar PV	10	10	$2,637	25.0%	25.0%

Table 5.5. Optimum combination of collector area and storage capacity for a minimum solar fraction of 50.0%

System type	Collector area (m^2)	Storage capacity (kWh)	Equivalent annual cost ($)	Solar fraction	% GHG reduction
Adsorption	40	40 (≈682 gallons)	$4,268	65.0%	30.4%
Absorption	30	45 (≈765 gallons)	$4,237	50.0%	33.8%
Solar PV	20	30	$4,122	53.3%	53.3%

Chapter 6: Conclusions and future work

The world is grappling with two serious issues related to energy and climate change. Air-conditioning plays a vital important role in both. While the common refrigerants utilized in the conventional air-conditioning systems contributes to global-warming, a primary reason for the climate change, the higher temperatures lead to greater air conditioning use, creating a positive feedback. Research and development of alternative forms of air-conditioning systems is extremely important to break this vicious cycle. The research reported in this dissertation has attempted to investigate feasibility of small-scale thermal-powered adsorption cooling systems. A novel bench-scale adsorption system prototype using a novel adsorbent-refrigerant pair of activated carbon and butane was developed and experiments conducted. Also, numerical simulations were conducted to compare thermo-economic performance of various solar powered air conditioning systems based on the solar collector size and storage capacity. The conclusions and suggested future works are as follows:

6.1. Conclusions

From the simulation results comparing the adsorption, the absorption, and the desiccant system, it is shown that adsorption and absorption system provides similar cooling output except the fact that only adsorption system can operate at generation temperatures below 65 ^{o}C. This is an important result because temperatures in this range can be

provided by flat-plate solar collectors, an inexpensive type of thermal collectors. But, it was also found that an adsorption system is less efficient (low COP) than a comparable absorption system. The performance of a desiccant system is in the middle of these two systems but its inability to operate in certain ambient conditions makes it an unlikely future solution. Further comparisons were made based on the available system size, specific cooling power, maturity of technology, and safety of operation. Except having lower specific cooling power, adsorption systems were found to be a better option.

To further investigate the feasibility of small-scale adsorption cooling systems, a bench-scale prototype was developed and tested. The prototype employed a novel design to accomplish heat and mass recovery and improved heat transfer throughout the adsorber chamber. Additionally, a novel adsorbent-refrigerant pair of activated carbon and butane is used. The cooling capacity of the prototype was estimated to be about 89.6 W and tested COP was about 0.12. Although, COP was lower compared to other larger systems reported in the literature (typical COP ranges between 0.3-0.7), it was still considered a relative success due to first such known attempt on small-scale adsorption system. The design also had few shortcomings, particularly in the sealing of the system. The system developed leaks with-in a short interval after being exposed to heat at brazed joints of adsorber vessel and heat transfer tubes.

The final analysis undertaken in this work was to compare the thermo-economic performance of different solar-powered heat pump systems for a single-family residential household in Phoenix, AZ. An energy simulation model was developed in eQUEST to estimate the hourly cooling and heating load. The thermal performance comparison was based on the solar fraction (% solar contribution to the total load) for various sizes of solar collector area and storage capacity. It is shown that a solar photovoltaic powered vapor compression system provides the highest solar fraction in comparison to solar thermal powered adsorption and absorption system for collector area of 50 m^2 and exergy storage capacity of 25 kWh. The solar fraction increases by increasing the collector size and the storage capacity. However, there exists a point after which increasing the storage size for a fixed collector area and vice versa ceases to have any impact on the solar fraction.

The economic comparison based on the equivalent annual cost has shown that operating a thermal system is slightly better for 50 m^2 collector area and 25 kWh exergy storage capacity. This is due to relatively higher cost of solar PV arrays and battery storage. It is also shown that at a fixed solar collector area of 50 m^2, an absorption system is more economical below 20 kWh exergy storage capacity and adsorption system above 20 kWh. For a fixed exergy storage capacity of 25 kWh, the solar electric system fares better below 30 m^2 solar collector area, absorption system between 30 – 40m^2, and adsorption system for larger than 40m^2 solar

collector area. The optimum combination of collector area and exergy storage capacity is also determined for each system.

6.2. Future work

Experimental works in this study have shown some potential for small-scale adsorption cooling system. Also, numerical simulations have shown their suitability at lower generation temperatures and economic equanimity compared to other competitive solar technologies. The following questions, however, should be addressed in future work:

1. Heat transfer between the adsorbent particles in the adsorber and at the interface of adsorbent and heat exchange should be improved in order to reduce the volume of the adsorption chiller. The present work made an attempt by distributing the heat exchanger tubes throughout the adsorber to reduce the effective conductance length. However, further research is required in either finding new adsorbent material with high-thermal conductivity and/or other innovative heat transfer schemes. Further, a real-life size experimental system must be built and tested to get more in-sight in the actual system performances.
2. The thermo performance analysis presented in Chapter 5 assumed constant COP for all three systems whereas solar system performance and building load was calculated on hourly basis for one year period. The next step in the analysis to have the complete system coupled dynamically and simulation is done for 8,760 hours to predict the system performance. Additionally, the analysis restricts the available

solar hot water/ electricity to the cooling and heating needs and any excess capacity particularly during winter months is wasted. However, further improvements in the model can be made where any excessive hot water can be utilized for other end-use (such as shower, dish-washer etc.) and electricity for lighting purpose or to sell back to the utility.

References

[1] B. Anderson, Solar energy: fundamentals in building design, McGraw-Hill Book Co., Chapter 1-A (1977) 3-9.

[2] W. Cullen, Of the cold produced by evaporating fluids and of some other means of producing cold, in essays and observations Physical and Literary read before a society in Edinburgh and published by them, II (1756).

[3] W.H. Carrier, History and development of air conditioning industry, Refrigeration 1 (1933) 18-21.

[4] G. B. Wilson, Air conditioning being a short treatise on the humidification, ventilation, cooling and the hygiene of textile factories – especially in relation to those in the U.S.A. John Wiley & Sons, New York (1908), As reported in Donaldson and Nagengast (1994).

[5] M. Jones, Air conditioning, Newsweek Special (1997) 42-43.

[6] F.S.Rowland, M.J. Molina, Stratospheric for Chlorofluoromethanes: Chlorine atom-catalyzed destruction of ozone, Nature 249 (1974) 810-812.

[7] United Nations Environment Programme, Montreal protocol on substances that deplete the ozone layer, Final Act United Nations, New York, U.S.A.

[8] J. Hansen. et al., Dangerous human-made interference with climate: a GISS modelE study, *Atmos. Chem. Phys* 7 (2007) 2287-2312.

[9] Y. Fan, L. Luo, B. Souri, Review of solid sorption refrigeration technologies: development and applications, Renewable and Sustainable Energy Reviews 11 (2007) 1758-1775.

[10] B.A. Carreras, D. E. Newman, I. Dobson, A. B. Poole, Evidence for self-organized criticality in a time series of electric power system blackouts, IEEE Transactions on Circuits and Systems I: Regular Paper 51 (2004) 1733-1740.

[11] P. Hines, Trends in the history of large blackouts in the United States, Power Engineering Society, IEEE General Meeting (2008) 1-8.

[12] 2002-2012 Electricity outlook report, Pub. 700-00-004F, California Energy Commission (2002).

[13] J. Michals, E. Titus, The need for and approaches to developing common protocols to measure, track, and report energy efficiency savings in the Northeast, Proceedings of the 2006 ACEEE Summer Study, Washington, DC: American Council for an Energy-Efficient Economy (2006) 8–179 to 8–190.

[14] R. Best, N. Ortega, Solar refrigeration and cooling, Renewable Energy 11 (1999) 685-690.

[15] J. M. Gorden, K.C. Ng, High-efficiency solar cooling, Solar energy 68 (2000) 23-31.

[16] G.A. Florides, S.A. Tassou, S.A. Kalogirou, L.C. Wrobel, Review of solar and low energy cooling technologies for buildings, Renewable and Sustainable Energy Reviews 6 (2002) 557-572.

[17] A.M. Papadopoulos, S. Oxizidis, N. Kyriakis, Perspectives of solar cooling in view of the developments in the air-conditioning sector, Renewable and Sustainable Energy Reviews 7 (2003) 419-438.

[18] H-M Henning, Solar assisted air conditioning of buildings—an overview, Applied Thermal Engineering 27 (2007) 1734-1749.

[19] Y. Hwang, R. Radermacher, A.A. Alili, I.Kubo, Review of solar cooling technologies, HVAC&R Research 14 (2008) 507-528.

[20] X.Q. Zhai, R.Z. Wang, A review of absorption and adsorption solar cooling systems in China, Renewable and Sustainable Energy Reviews 13 (2009) 1523-1531.

[21] M.K. Ewert, M. Agrella, D. Demonbrun, J. Frahm, D.J. Bergeron, D. Berchowitz, Experimental evaluation of a solar PV refrigerator with thermoelectric, Stirling, and vapour compression heat pumps, In: Proceedings of ASES Solar Conference, Albuquerque, USA (1998).

[22] M. A. Green, K. Emery, D. L. King, Y. Hishikawa, W. Warta, Solar cell efficiency tables (version 29), Progress in Photovoltaics: Research and Applications 15 (2007) 35–40.

[23] R. Rudischer, J. Waschull, W. Hernschier, C. Friebe, Available solar cooling applications for different purpose, In Proceedings of

International Conference Solar Air Conditioning, Bad Staffelstein, Germany (2005).

[24] P. Srikhirin, S. Aphornratana, S. Chungpaibulpatana, A review of absorption refrigeration technologies, Renewable and Sustainable Energy Reviews 5 (4) (2001) 343-372.

[25] K. Sumathy, K.H. Yeung, L. Yong, Technology development in the solar adsorption refrigeration systems, Progress in Energy and Combustion Science 29 (2003) 301–327.

[26] D.S. Kim, C.A. Infante Ferreira, Solar refrigeration options – a state-of-the-art review, International Journal of Refrigeration 31 (2008) 3-15.

[27] C.A. Balaras et al., Solar air conditioning in Europe –an overview, Renewable and Sustainable Energy Reviews 11 (2007) 299-314.

[28] X. Liao, R. Radermacher, Absorption chiller crystallization control strategies for integrated cooling heating and power systems, International Journal of Refrigeration 30 (5) (2007) 904-911.

[29] K. Daou, R.Z. Wang, Z.Z. Xia, Desiccant cooling air conditioning: a review, Renewable and Sustainable Energy Reviews 10 (2006) 55-77.

[30] A. Kodama, M. Ohkura, T.Hirose, M. Goto, H. Okan, An energy flow analysis of a solar desiccant cooling equipped with a honeycomb adsorber, Adsorption 11 (1) (2005) 597-602.

[31] L. Harriman, Application engineering manual for desiccant systems, a report prepared for American Gas Cooling Center (1996).

[32] B.B. Saha, A. Akisawa, T. Kashiwagi, Solar/waste heat driven two-stage adsorption chiller: the prototype, Renewable Energy 23 (2001) 93- 101.

[33] M.A. Lambert, B.J. Jones, Review of regenerative adsorption heat pumps, Journal of Thermophysics and Heat Transfer 19 (4) (2005) 471-485.

[34] D. M. Ruthven, Principles of adsorption and adsorption processes, New York, Wiley (1984).

[35] M. Suzuki, Adsorption for energy transport, Adsorption Engineering, Japan (1980).

[36] D.D. Duong, Adsorption analysis: equilibria and kinetics, Series on Chemical Engineering, Imperial College Press 2 (1998) 13-15.

[37] E.E. Anyanwu, Review of solid adsorption solar refrigeration II: an overview of the principle and theory, Energy Conversion and Management 45 (7-8) (2004) 1279-1295.

[38] R. Plank, J. Kuprianoff, Die Kleinkältemaschine, Springer, Berlin (1960).

[39] G.E. Hulse, G.E. Freight, Car refrigeration by an adsorption system employing silica- gel, Refrig. Engnr 17 (1929).

[40] E.B. Miller, The development of silica gel refrigeration, Am. Soc. Refrig. Engnr 17 (1929).

[41] F. Meunier, Etude des couples adsorbante-solide refrigerant liquide, EEC Report, EUR, 7707.

[42] D.I. Tchernev, D.T. Emerson, High-efficiency regenerative zeolite heat pump, ASHRAE Transactions 94 (2) (1988) 2024-2032.

[43] B.B. Saha, E.C. Boelman, T. Kashiwagi, Experimental investigation of a silica gel-water adsorption refrigeration cycle-the influence of operating conditions on cooling output and COP, ASHARAE Transactions 101 (2) (1995) 358-366.

[44] D.J. Miles, S.V. Shelton, Design and testing of a solid-sorption heat pump system, Applied Thermal Engineering 16 (1996) 389-394.

[45] R.Z. Wang, Performance improvement of adsorption cooling by heat and mass recovery operation, International Journal of Refrigeration 24 (2001) 602-611.

[46] X.J. Zhang, R.Z. Wang, A new combined adsorption-ejector refrigeration and heating hybrid system powered by solar energy, Applied Thermal Engineering 22 (11) (2002) 1245-1258.

[47] Y.L. Liu, R.Z. Wang, Z.Z. Xia, Experimental performance of a silica gel-water adsorption chiller, Applied Thermal Engineering 25 (2-3) (2005) 359-375.

[48] D.C. Wang, Z.Z. Xia, J.Y. Wu, R.Z. Wang, H. Zhai, W.D. Dou, Study of a novel silica gel-water adsorption chiller part I: design and performance prediction, International Journal of Refrigeration 28 (7) (2005) 1073-1083.

[49] E. Sharkawy, K. Kuwahar, B.B. Saha, S. Koyama, K.C. Ng, Experimental investigation of activated carbon fibers/ethanol pairs for adsorption cooling system application, Applied Thermal Engineering 26 (8-9) (2006) 859-865.

[50] Y. Huangfu, J.Y. Wu, R.Z. Wang, Z.Z. Xia, Experimental investigation of adsorption chiller for micro-scale BCHP system application, Energy and Buildings 39 (2007) 120-127.

[51] M.A. Lambert, Design of solar powered adsorption heat pump with ice storage, Applied Thermal Engineering 27 (8-9) (2007) 1612-1628.

[52] M.O. Abdullah, J. L. Ngui, K. A. Hamid, S. L. Leo, S. H. Tie, Cooling performance of a combined solar thermoelectric-adsorption cooling system: an experimental study, Energy Fuels 23 (2009) 5677-5683.

[53] X.Q. Zhai, R.Z. Wang, Experimental investigation and theoretical analysis of the solar adsorption cooling system in a green building, Applied Thermal Engineering 29 (1) (2009) 17-27.

[54] N. D. Banker, M. Prasad, P Dutta, K. Srinivasan, Development and transient performance results of a single stage activated carbon – HFC 134a closed cycle adsorption cooling system, Applied Thermal Engineering 30 (10) (2010) 1126-1132.

[55] A. Freni, A. Sapienza, I.S. Glaznev, Y.I. Aristov, G. Restuccia, Experimental testing of a lab-scale adsorption chiller using a novel selective water sorbent “silica modified by calcium nitrate, International Journal of Refrigeration, In-Press.

[56] B.B. Saha, E.C. Boelman, T. Kashiwagi, Computer simulation of a silica gel water adsorption refrigeration cycle-the influence of operating conditions on cooling output and COP, ASHARAE Transactions 101 (2) (1995) 348-357.

[57] H.T. Chua, K.C. Ng, A. Malek, T. Kashiwagi, A. Akisawa, B.B. Saha, Modeling the performance of two-bed, silica gel-water adsorption chillers, International Journal of Refrigeration 22 (1999) 194-204.

[58] K. Chihara, M. Suzuki, Air drying by pressure swing adsorption, J Chem Eng Japan, 16 (4) 1983, 293-98.

[59] M.R.A. Afonso, V.J. Silveira, Characterization of equilibrium conditions of adsorbed silica-gel/water bed according to Dubinin-Astakhov and Freundlich, Thermal Engineering 4 (1) (2005) 3-7.

[60] L.Z. Zhang, A three-dimensional non-equilibrium model for an intermittent adsorption cooling system, Solar Energy 69 (1) (2000) 27-35.

[61] TIAX LLC, Review of thermally activated technologies, A distributed energy program report for the US DOE, Office of energy efficiency and renewable energy (2004).

[62] M.H. Henning, Air-conditioning with solar energy, SERVITEC meeting, Barcelona (2000).

[63] D.J. Miles, D.M. Sanborn, G.A. Nowakowski, S.V. Shelton, Gas-fired sorption heat pump development, Heat Recovery Systems and Combined Heat & Power 13 (4) (1993) 347–351.

[64] N. B. Amar, L.M. Sun, F. Meunier, Numerical analysis of adsorptive temperature wave regenerative heat pump, Applied Thermal Engineering 16 (5) (1996) 405–418.

[65] M. Pons, D. Laurent, F. Meunier, Experimental temperature fronts for adsorptive heat pump applications, Applied Thermal Engineering 16 (5) (1996) 395–404.

[66] X. Wang, H.T. Chua, K.C. Ng, Experimental investigation of silica gel-water adsorption chiller with and without a passive heat recovery scheme, International Journal of Refrigeration 28 (2005) 756-765.

[67] K. Oertel, M. Fischer, Adsorption cooling system for cold storage using methanol/silica gel, Applied Thermal Engineering 18 (9-10) (1998) 773-786.

[68] D.C. Wang, Z.Z. Xia, J.Y. Wu, Design and performance prediction of a novel zeolite-water adsorption air conditioner, Energy Conversion and Management 47 (2006) 590-610.

[69] R.Z. Wang, J.Y. Wu, Y.X. Xu, A continuous heat regenerative adsorption refrigerator using spiral plate heat exchanger as adsorbers, Applied Thermal Engineering 18 (1-2) (1998) 13-23.

[70] F. Lemmini, A. Errougani, Building and experimentation of a solar powered adsorption refrigerator, Renewable Energy 30 (2005) 1989-2003.

[71] W. Zhu, J.C. Groen, F. Kapteijn, J.A. Moulijn, Adsorption of butane isomers and SF_6 on Kureha activated carbon:1. Equilibrium, Langmuir 20 (2004) 5277 – 5284.

[72] U.S. Energy Information Administration, Residential Energy Consumption Survey 2001, http://www.eia.doe.gov/emeu/recs/contents.html, 2001 (accessed December 15, 2006).

[73] S. Ayyash, An assessment of the feasibility of solar absorption and vapor compression cooling systems, Energy Conversion and Management 21 (1981) 163-169.

[74] S. Ayyash, M. Sartawi, Economic comparison of solar absorption and photovoltaic-assisted vapour compression cooling systems, International Journal of Energy Research 7 (1983) 279-288.

[75] Elsafty, A. J. Al-Daini, Economical comparison between a solar-powered vapour absorption air-conditioning system and a vapour compression system in the Middle East, Renewable Energy 25 (2002) 569-583.

[76] S.A. Klein, D.T. Reindl, Solar refrigeration, *ASHRAE Journal* 47 (2005) 526-530.

[77] X.Z. Casals, Solar cooling economic considerations: centralized versus decentralized options, Journal of Solar Energy Engineering 128 (2006) 231-236.

[78] R.Z. Wang, T.S. Ge, C.J. Chen, Q. Ma, Z.Q. Xiong, Solar sorption cooling systems for residential applications: options and guidelines, International Journal of Refrigeration 32 (4) (2009) 638-660.

[79] K.F. Fong, T.T. Chow, C.K. Lee, Z. Lin, L.S. Chan, Comparative study of different solar systems for buildings in subtropical city, Solar Energy 84 (2010) 227–244.

[80] James J. Hirsch & Associates, “eQUEST the quick energy simulation tool,” http://doe2.com/equest/ (accessed February 16, 2011).

[81] Thermal environmental conditions for human occupancy, ASHRAE Standard 55-2004, Atlanta, GA: American Society of Heating, Refrigerating and Air-Conditioning Engineers.

[82] National Renewable Energy Laboratory, “National Solar Radiation Data Base: 1961-1990 Typical Metrological Year 2,” http://rredc.nrel.gov/solar/old_data/nsrdb/1961-1990/tmy2/, (accessed July 28, 2011).

[83] J.A. Duffie, W.A. Beckman, Solar Engineering of Thermal Processes, 3rd ed., Wiley (2006).

[84] Apricus Solar Collector Information Booklet, http://www.ch-ce.com/images/APRICUS_SOLAR_HOT_WATER.pdf (accessed August 01, 2011).

[85] Alternative Energy Technologies, “Solar collector certification and rating,” http://www.aetsolar.com/literature/SRCC_100-2002-001F.pdf (accessed August 01, 2011)

[86] York Heating and Air Conditioning, “LX Series YHJD Model,” http://www.yorkupg.com/homeowners/pdfs/Y_LX_YHJD_13_HP_SS.pdf (accessed July 28, 2011).

[87] National Renewable Energy Laboratory, “PVWatts,” http://www.nrel.gov/rredc/pvwatts/ (accessed December 15, 2010).

[88] B.S. Borowy, Z.M. Salameh, Methodology for optimally sizing the combination of a battery bank and PV array in a wind/PV hybrid system, IEEE Transactions on Energy Conversion 11 (2) (1996) 367-375.

[89] U.S. Energy Information Administration, “Solar thermal collector manufacturing activities, Table 2.12 (updated Jan., 2011),” http://www.eia.doe.gov/cneaf/solar.renewables/page/solarreport/solar.html (accessed July 10, 2011).

[90] Plastic-Mart, http://www.plastic-mart.com/search.aspx?search=hot%20water%20tank (accessed July 31, 2011).

[91] SunMaxx Solar, http://www.sunmaxxsolar.com, quote received by email on May 02, 2011 for 512 and 1,160 gallon storage tanks.

[92] T. Tsoutsos, E. Aloumpi, Z. Gkouskos, M. Karagiorgas, Design of a solar absorption cooling system in a Greek hospital, Energy and Buildings 42 (2010) 265-272.

[93] The European PV Technology Platform, Projection of PV system prices: Australia, Europe, Japan, USA 2004-2030, PV Platform Working Group 2 (2003).

[94] Navigant Consulting, Inc., A review of PV inverter technology cost and performance projections, National Renewable Energy Laboratory, NREL/SR-620-38771 (2006).

[95] Itron, Inc., CPUC self-generation incentive program-solar PV costs and incentive factors (2007).

[96] D. Ton, G.H. Peek, C. Hanley, J. Boyes, Solar energy grid integration systems – Energy Storage (SEGIS-ES), Sandia National Laboratories (2008).

[97] Database for Energy Efficiency Resources version 2008.2.05, Developed by the California Public Utilities Commission, http://www.deeresources.com (accessed August 2, 2011).

[98] U.S. Energy Information Administration, Natural gas explained: natural gas prices, http://www.eia.gov/energyexplained/index.cfm?page=natural_gas_prices (accessed August 2, 2011).

[99] U.S. Energy Information Administration, Electricity explained: factor affecting electricity prices, http://www.eia.gov/energyexplained/index.cfm?page=electricity_factors_affecting_prices (accessed August 2, 2011).

[100] H. Arkin, R. Navon, Thermodynamic aspects of selecting an economical domestic cooling system for desert areas, ASHRAE Transactions 100 (2) (1994) 329-338.

[101] E.H. Pechan & Associates, The emissions & generation resource integrated database for 2010 (Year 2007 eGRID subregion emissions - greenhouse gases),Prepared for U.S. Environmental Protection Agency (2010).

[102] Energy Information Administration, Documentation for emissions of greenhouse gases in the United States 2005, DOE/EIA-0638, (2007) 181.

APPENDIX A

ACTIVATED CARBON DATA SHEET

Norit Activated Carbon

leading in purification

ISO 9001:2000
FM 25618

DATASHEET

No. 3361
Sep 2007

SORBONORIT® 4

EXTRUDED ACTIVATED CARBON

SORBONORIT 4 is a steam activated extruded carbon with a diameter of 4 mm. It is a carbon with superior mechanical hardness that is excellent for solvent recovery applications.

Product Specifications

Butane adsorption at p/p_o = 0.1, g/100 g	26-28
Apparent density, kg/m^3	360-400
Moisture (as packed), mass-%	5 max.

Typical Properties

Butane adsorption at p/p_o = 0.42, g/100 g	31
Butane adsorption at p/p_o = 0.01, g/100 g	20
Benzene adsorption at p/p_o = 0.1, g/100 g	42
Carbon tetrachloride activity, g/100 g	80
Surface area (BET), m^2/g	1400
Ball-pan hardness	99
Particle size	
> 3.35 mm, mass-%	99
Ash, mass %	7
Ignition temperature, °C	≥ 490

NOTES

1) All analyses based on NORIT Standard Test Methods (NSTM).
2) Typical properties for general information only, not to be used as purchase specifications.

Packaging/Transportation

Standard package is 20 kg bags, 40 bags per pallet for a net pallet weight of 800 kg.
Activated carbon (NOT REGULATED)
Exempt from DOT, IATA, and IMDG regulations
Import/Export classification: 3802.10.0000 (HS Tariff Classification)
Domestic Freight Classification: NMFC 040560
CAS # 7440-44-0

Material Handling

Wet activated carbon depletes oxygen from air and, therefore, dangerously low levels of oxygen may be encountered. Whenever workers enter a vessel containing activated carbon, the vessel's oxygen content should be determined and work procedures for potentially low oxygen areas should be followed. Appropriate protective equipment should be worn. Avoid inhalation of excessive carbon dust. No problems are known to be associated in handling this material. This product may contain silica. Please see the product Material Safety Data Sheet for details. Long-term inhalation of high dust concentrations can lead to respiratory impairment. Use forced ventilation or a dust mask when necessary for protection against airborne dust exposure (see Code of Federal Regulations - Title 29, Subpart Z, par. 1910.1000, Table Z-3).